Performance Characterization and Optimization of an Axial Flow Fan for Electronic Enclosures

A Thesis

by

Hafiz M. Hashim

Submitted to the
Graduate School of Science and Engineering
In partial fulfillment of the requirement for
The degree of

Master of Science (M.Sc.)

In the
Department of Mechanical Engineering

Özyeğin University
March, 2016.

Copyright ©2016 by ***Hafiz M. Hashim***

Performance Characterization and Optimization of an Axial Flow Fan for Electronic Enclosures

Approved by:

Associate Professor Mehmet Arik,
Advisor
Department Mechanical,
Engineering
Özyeğin University

Assistant Prof Dr. Altug Basol
Department of Mechanical,
Engineering
Özyeğin University

Associate Prof. Dr. Erkan Mese
Department of Electrical & Electronics,
Engineering
Yildiz Technical University

Date Approved: 2016.

To my family, friend and teacher

ABSTRACT

Thermal management of high power electronic components have become a challenging and critical issue for thermal engineers. Forced convection electronic enclosures comprises of fans to provide fluid flow through the system to remove heat efficiently. In this study, performance characterization of an axial fan for electronic enclosures has been performed computationally and experimentally. For this purpose, by using the three-dimensional CAD model of a fan with Computational Fluid Dynamics (CFD) are evaluated in comparision with the experimental data. An experimental system was designed and built for the validation of numerical models. All the measurements were carrried out in a wind tunnel which was designed and manufactured according to the Air Movement Control Assosciation (AMCA) standard 210-99, 1999.

In order to make relevant comparisions, a detailed computational model of the wind tunnel setup along with the fan were modeled. Moving Reference Frame (MRF) technique is used for the modelling of an axial fan and the simulations were performed by utilizing realizable k–ε turbulence model with enhanced wall function to determine flow and pressure fields over a range of flow rates. Experimental investigation in the wind tunnel by measuring the pressure rise and flow rate through the fan by using multiple nozzles which was also designed and manufactured according to the Air Movement Control Assosciation (AMCA) standard 210-99, 1999. Understanding of the overall fan efficiency as a function of the volumetric flow rate and th improvement concerning with the losses occur across the fan are described.

In the second phase of the study, power losses of an axial fan are investigated to determine the effect different components on the overall efficiency. Moreover, it deals

with the modeling of mechanical, electrical, thermal and electromagnetic losses which focus especially on an outer rotor brushless DC motor. Efficiency of a fan depends on its electrical and mechanical designs as well as the environmental conditions that the fan is exposed to. Typically, the overall efficiency of an axial fan varies between 15 to 40 percent. Power losses may be due to electrical, aerodynamic or mechanical design components. Losses occurring in an axial fan motor have become a critical issue in which high inertial effects, low power, low cost and high efficiency are desired. In order to design an efficient motor, it is important to accurately predict the power losses which are usually dissipated in the form of heat. Reduction of these losses leads to a decrease in the motor temperature and, therefore, has a positive effect on the fan reliability. Expressions for calculating the inverter losses, motor losses and mechanical losses are derived. The power losses obtained are then used as heat sources when evaluating the thermal performance of the motor. By using a two-dimensional model, computational fluid dynamics (CFD) simulations are performed to analyze the core loss distribution across the motor. The results are utilized to determine evaluate the overall efficiency of the system.

ÖZETÇE

Yüksek güçlü elektronik komponentlerin ısıl yönetimi, termal mühendisler için zorlayıcı ve kritik bir problem haline gelmiştir. Zorlanmış taşınımlı elektronik mahfazalar, sistemdeki ısıyı verimli bir şekilde ortadan kaldırmak için akış yaratan fanlardan oluşmaktadır. Bu çalışma kapsamında, elektronik mahfazalarda kullanılan eksenel bir fanın performans karakterizasyonu üzerine sayısal ve deneysel çalışmalar gerçekleştirilmiştir. Bu amaç ile bir fanın üç boyutlu CAD modeli kullanılarak hesaplamalı akışkanlar dinamiği ile deneysel veriler ile karşılaştırılması yapılmıştır. Sayısal modellerin doğrulamasını yapmak amacıyla bir deneysel düzenek tasarlanmış ve kurulmuştur. Tüm ölçümler, Air Movement and Control Association (AMCA- Hava Hareket ve Kontrol Kurumu) 210-99,1999 standardına uygun olarak tasarlanmış ve üretilmiş bir rüzgar tüneli içerisinde gerçekleştirilmiştir.

Tutarlı karşılaştırmalar yapmak adına, fan ile birlikte rüzgar tüneli düzeneğinin sayısal modeli hazırlanmıştır. Eksenel bir fanın modellemesi sırasında Hareketli Referans Çerçevesi (Moving Reference Frame) tekniği kullanılır. Akış hızları aralığı üzerine, akış ve basınç alanlarına karar vermek için geliştirilmiş duvar fonksiyonu ile gerçekleştirilebilir k–ε türbülans modeli kullanılarak simülasyonlar yapılmıştır. Rüzgar tünelinde yapılan deneysel araştırmalar, fandan kaynaklanan basınç artışı ve akış hızı ölçülerek tamamlanmıştır. Bu ölçümler sırasında AMCA 210-99, 1999 standardına uygun olarak tasarlanmış ve üretilmiş birden fazla çıkış ağzı (nozzle) kullanılmıştır. Fanın toplam verimlilik kavramı, hacimsel debiye ve fan boyunca oluşan kayıplar ile ilgili gelişmelere bağlı bir fonksiyon olarak tanımlanmaktadır.

Çalışmanın ikinci fazında, farklı komponentlerin genel verim üzerindeki etkisini görmek amacıyla eksenel fanın güç kayıpları araştırılmaktadır. Dahası, güç kayıpları özellikle fırçasız doğru akım motorunun dış rotoruna odaklı mekanik, elektriksel, termal ve elektromanyetik kayıpların modellemesi ile bağlantılıdır. Bir fanın verimliliği, elektriksel ve mekanik tasarımına bağlı olmakla birlikte fanın maruz kaldığı çevre koşullarına da bağlıdır. Genellikle, bir eksenel fanın

toplam verimliliği %15 ila %40 arasında çeşitlilik göstermektedir. Güç kayıpları; elektriksel, aerodinamik veya mekanik tasarım parçalarından kaynaklanabilir. Yüksek atalet etkisi, düşük güç, düşük maliyet ve yüksek verim beklendiğinde, eksenel fanlar üzerinde oluşan kayıplar kritik bir problem haline gelir. Verimli bir motor tasarlamak için genellikle ısı formunda oluşan güç kayıplarını doğru olarak öngörmek önemlidir. Bu kayıpların giderilmesi motor sıcaklığının düşmesine yol açar ve bu sayede, fanın güvenilirliğini arttırır. Evirici kayıpları, motor kayıpları ve mekanik kayıpları hesaplamak için formüller türetilmiştir. Güç kayıpları belirlenmiş ve sonra motorun termal performansını değerlendirmek için güç kaynağı olarak kullanılmıştır. İki boyutlu bir model kullanılarak, motor üzerindeki çekirdek kaybı dağılımını analiz edebilmek amacı ile hesaplamalı akışkanlar dinamiği (HAD) simülasyonları üzerine çalışılmıştır. Sonuçlar, sistemin genel verimliliğine karar verebilmek için kullanılmıştır.

ACKNOWLEDGEMENT

Financial support for the research project was provided by an ASELSAN A.Ş. and Turkish Undersecretariat for Defense Industries (SSM).

I would like to express my gratitute to my supervisor Associate Professor Dr. Mehmet Arik for his invaluable guidance and support towards my research. It has been a great learning experience working with him. I would like to express my deppest gratitude towards him for offering instructive suggestions at all times. I would also like to thank Dr. Baris Dogruoz from CISCO and Murat Parlak from ASELSAN being collaborators of this project.

Last, but not least I offer sincere thank to my family especially my mother for her precious support throughout my graduate school journey and members of ARTgroup for their kindness and support during my M.Sc. study at Ozyegin University.

TABLE OF CONTENTS

LIST OF FIGURES

LIST OF TABLES

NOMENCLATURE

P	Pressure	(N/m^2)
f	Frequency	(Hz)
D	Fan diameter	(m)
d	Orifice/nozzle diameter	(m)
V	Applied voltage	$(Volts)$
K	Loss coefficient	
m	Mass	(kg)
t	time	(s)
T	Temperature	(K)
T_{amb}	Ambient temperature	(K)
u	Velocity in x-direction	(m/s)
v	Velocity in y-direction	(m/s)
P	Power	$(Watt)$
Q	Volume flow rate	(m^3/s)
Re	Reynolds number	
I	Current	(A)
G	Weight	(N)
N	Speed	(rpm)
R	Resistance	(ohm)
τ	Torque	$(N\text{-}m)$
c	Chord	(m)
x	Camber location	(m)

t	Thickness	*(m)*
AR	Aspect ratio	
V	velocity	*(m/s)*
B	span	*(m)*
K	pressure rise coefficient	
C	Coefficient	
A	Area	(m^2)
d	Nozzle diameter	*(m)*
e	Per unit uncertainty	

Greek Symbols

μ	Kinematic viscosity	(m^2/s)
ρ	Density	(kg/m^3)
ω	Angular Speed	*(rad/s)*
η	Fan Efficiency	*(%)*
θ	Blade twist angle	*(degree)*
β	Flow angle	*(degree)*
α	Angle of attack	*(degree)*
ε	Swirl coefficient	
λ	Flow coefficient	
β	Contraction ratio	
Y	Expansion factor	

Subscript

f	Fan

h	Hub
r	Rotational
st	Stagnation
sw	Switch
ph	Phase
in	Input
rot	Rotor
fr	Friction
cond.	Conduction
e	Eddy
h	Hysteresis
t	Throat
d	Discharge
n	Nozzle
rms	Root mean square
a	Armature
int.	Inverter
g	Fan pressure
m	Maximum

CHAPTER I

INTRODUCTION

Overview of Axial Fan Technology

Axial fan technology is heavily utilized for electronics cooling in military and commercial applications which drives the air through the fan rotor in estimation of an axial direction with lower pressure rise and the large mass flow rate characteristics. Forced convection-cooling fans which can be axial or radial, small or large in many different configurations which provide fluid flow efficiently in order to remove heat through the cooling systems.

Figure 1: Axial fans for electronic enclosures [1].

The actual characteristics of an axial fan mainly depend on its aerodynamic design and number of blades, also the angle at which blades are installed to approach airstream. The aerodynamic losses largely occur due to the integral pressure difference between the pressure and suction side of blade, which also contributes towards the noise generation and it's considered to be a major energy loss mechanism in axial fan systems. Efficiency of a fan depends on electrical and mechanical designs as well as environmental conditions

where it may vary between 15 to 40 percent. An axial fan's working principle is to transfer energy between the working fluid and the rotor. The rotor is comprising of blades with a definite profile so the fluid flow between blades in order to execute a particular force on the fan blades. Stators are also used in fans to drive the fluid smoothly. Owing to its multifunctional nature, the axial fans have been widely adopted in many applications.

Design of an axial fan for achieving the highest possible efficiency, high performance and reduction in power losses have turn into a mainstream in the advancement of axial fan technology. Axial fans are usually characterized by the fan performance curve which represents the relation between the static pressure and the fan volume flow rate, generally dictates the overall efficiency of the fan system. So there should be a moderate velocity and pressure profile as all these parameters are co-related. Power losses in an axial fan mainly consist of aerodynamic and motor losses where the former is usually acquainted with fan blades and casing of the fan and the latter is related to core losses, inverter losses and frictional losses. As all these mechanical and electrical power losses occur across the fan need to be characterized and optimize which ultimately affect the overall efficiency of the complete fan system. In this study, performance characterization of an axial fan has been carried out both mechanically and electrically in order to identify the factors which lead to the reduction in overall efficiency of the system.

Axial Fan Types

Axial fans can be classified into four types [2],

1. Propeller fans

2. Tubeaxial fans

3. Vaneaxial fans

4. Dual stage axial fans

Propeller fans: These are the most commonly used fans which can be utilized in in any kind of application or environment. These fans are generally used for ventilation applications where high flow rate with a minimal pressure rise are required. The efficiency of propeller fans is considered to be low compared to typical axial fans. Additionally, these fans are considered to be noisy. The drive system of propeller fans consists of either direct drive in which the motor is directly coupled to rotor or belt drive in which the belt is used to transmit the mechanical motion to the hub. Propeller fans are considered to be the lightest, less expensive and most commonly used fans for ventilation purposes. Propeller fans are designed in a way that they can transport considerable air volumes at low static pressures.

Propeller fans can be assembled into belt type configuration and direct type configuration. In belt configuration, belt and pulley are used to transfer the electrical energy into rotational energy to fan. Whereas, in direct type configuration, an electric motor installed directly to fan rotor. Belt type configuration shows more performance, since various rotational speeds can be achieved by selecting the suitable pulley ratio for the fan. Belt type configuration is usually prefer for larger size fans since it will maintain the speed of the fan while maintaining the motor speed high, from the cost perspective low speed motors with the same horse power are considered to be expensive than the high-speed motors [2]. Direct type configuration propeller fans are more efficient than the belt type configuration as it contains less number of components; require no maintenance and

results in lower cost, whereas in belt type propeller fans some power is consumed in the belt and pulley which results in high maintenance cost.

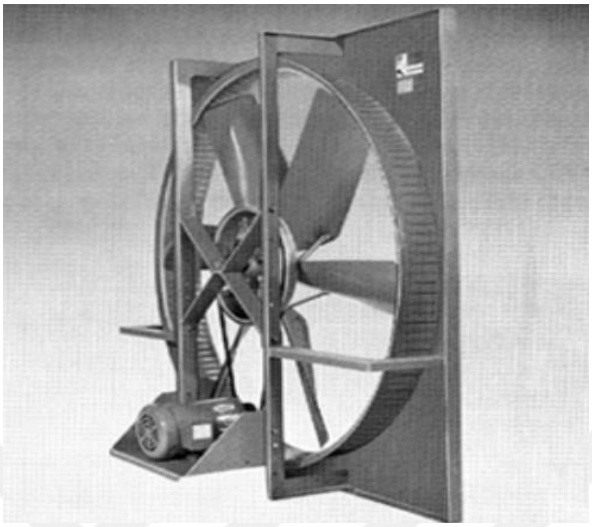

Figure 2: A belt type propeller fan [3]

Figure 3: A direct type propeller fan [3]

Tubeaxial fans: These fans are high speed fans and consist of a cylindrical housing. These fans can produce higher pressure rise and operate at improved efficiencies as compared to propeller fans. These kinds of fans are commonly used in the gas exhaustion systems. The hub diameter of tube axial fans is about 30% to 50% of the impeller

diameter. The main disadvantage of tubeaxial fans are the high noise level and frictional losses occur due to air spin in the fan outlet, which can be minimized about 10 % by using the venturi inlet instead of a duct. The vane axial fans have relatively higher cost compared to the propeller fans. The energy efficiency is about 65% [3]. These fans can be placed both at the inlet and outlet of the duct but usually due to the presence of air spin at the fan outlet tube axial fans are used at the inlet of the duct for the exhaust application.

Figure 4: A tube axial fan [3]

Vaneaxial fans: These fans comprise of casing like tubeaxial fans and guided vanes which reduces the effect of spinning air by eliminating the swirl component of the velocity in order to attain additional pressure rise. The casing of a vane axial fan consists of a converging tailpiece, set of guide vanes, an inner ring and an expanding diffuser in order to regain static pressure. The guide vanes present at the fan downstream are used to reduce the angular component of the air by deceleration and by transforming some of the glut velocity pressure into additional static pressure [4]. Vane axial fans can be used for blowing and exhausting purposes. The hub diameter of vane axial fans is usually 50% to 80% percent of the rotor diameter. Vane axial fans can generate high volumetric flow rates and relatively high-pressure rise as compared to other fans. Vane axial fans are used

where high static pressure is required. The overall efficiency of vane axial fan can be exceed to 85%.

Figure 5: Vane axial fan [3]

Dual stage axial fans: Dual stage axial fans are usually used where a high static pressure is required. Two-stage axial fan consist of dual fans which are coupled in series, so that the pressure rise occurs across each fan add up. These fans might also comprise of guide vanes in between the two rotors rotating in the direction of fans in order to smoothen the flow. There are two types of design exits in dual stage axial fan; first in which two counter rotating fans with no guide vanes and second with guide vanes in between the two fans rotating in the direction of fans. Both methods cause an increase in the static pressure. In the first type, the two counter rotating fans are operating by individual motors. The air spin occur at the first fan outlet is more or less defused by the deflection produced by the second fan. Due to this reason, guide vanes are not required in this method, which ultimately decreases the manufacturing cost and an additional benefit of this using this method is that if one motor fails, the system can still able to deliver some air by one stage running. In the second type, the guide vanes can obtain the swirl flow

occur due to the rotation of the first fan blades and converse the rotational component of the flow in the reverse direction for the intake of the second fan. The advantage of using two stage axial fans is that both fan stages can operate by utilizing the same rotor shaft with an adjustment on blades angles for the second fan.

Figure 6: Two-stage axial fan [3]

Fan blade

Fans, comprising of multiple rotating blades energized by an electric motor, are utilize to move air in a range of various residential and commercial applications. There are two main types of fans lies under are centrifugal fans and axial fans. Centrifugal fans have three further types, forward inclined blades, backward inclined blades and straight radial blades. The selection of the preferable fan type based on application requirements for air flow, pressure rise, size and space limitations and overall cost. Usually, fan selection is carried out by the application or cost, while energy efficiency is a secondary driver.

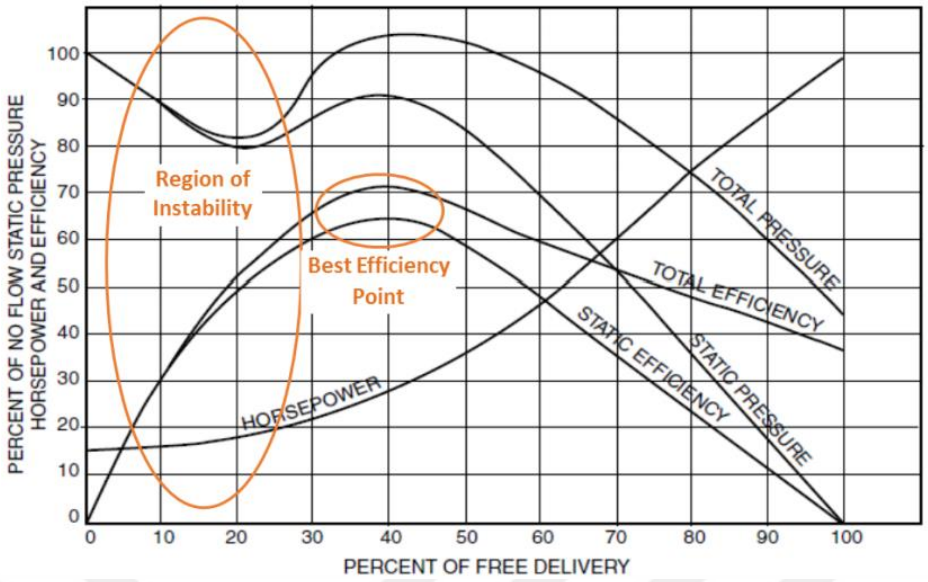

Figure 7: Fan performance characteristics

Figure shows the illustration of the overall performance in terms of different parameters with respect to percent of free delivery, this condition exists when there is are no active resistance to air flow (no static pressure) at the inlet or outlet of the fan. The designers objective for the system to operate at or nearly to the the best efficiency point (BEP), at which fan operates most effectively in terms of total efficiency (delivered pressure and airflow divided by power consumption) and maintenance considerations. Whereas, the fan operating at higher or lower free delivery percent will lead to low efficiency, increases equipment wear and fan noise.

Fans can have a instability region as shown in figure. Fan can results in dramatic increase in noise and vibration operating in instability region. continued operation in this region can cause unstable, pulsating airflow which lead to structural fatigue damage to the fan due to continuous loading and unloading of components and can cause damage to ductwork and other system components. A fan system may not be able to perform properly due to unsteady flow or transmitted vibration. In instability region, stall occurs when the fan is delivering flow which is too small for its predetermined design.

When the airflow passes through the fan blades, it deflects the air by means of angle of attack which can be increase or decrease by changing the orientation of the object relative to the flow direction which allows the fan to generate pressure . the stalling in the fan occur when the in-uniformity occur and the air is not able to follow the blade surface due to the severeness of attack angle. In a fan system, the blades are usually rotating with a constant velocity. Higher flow rates possess increased the attack angle and lower flow rates possess decreased angle of attack through the inlet.

In some of the fans, the angle of attack is not uniform across the width of the blade. These kinds of fan are not normally considered to be a most efficient fans, although the severity of the stall is often too small since only part of the blade is stalling at any one flow rate. Where research showed that radial bladed centrifugal fans are usually in stall due to the indigent match between the directional velocity of the blade and the approaching air. However, these fans may have varying flows at low flow rates since the internal losses are dictated by stall and the pressure drops at this point. The appropiate fan blade profile should be selected on the basis of highest acheivable efficiency which is with high lift and low drag on fan blade so that the fan blades can generate an aerodynamic lift that pressurizes the air.

Overview of Out-spin Brushless D.C. Motor Technology

Brushless DC motors have attained a greater attention in the global market because of their low cost and low power applications that require constant speed such as fans motors, motors used in printers and copiers etc. In general, brushless DC motors are advantageous in such applications where high inertia effects are beneficial to the system performance. Brushless DC motors are nowadays become as an interesting solution for variable speed

drives which are compatible with all ranges of inverters because of their feasibility for cooling applications. Since the brushless DC motor has the feature of reliability, quiet operation, small size, low maintenance and high efficiency. The crucial advantages of outer rotor motor in comparison with the inner rotor motor are the lower losses and higher torque density.

In a typical DC motor, the brushes are pledged for creating the mechanical interaction with a set of electrical interactions on the rotor with respect to the commutator which forms an electric circuit between the armature coil windings and the DC electrical source. As the armature rotates, the stationary brushes come in contact with the three different commutator segments and form a set of electrical switches, which operate in a sequence to allow electric current to flow through the armature coils nearest to the permanent magnet or electromagnet field [5]. On the other side, BLDC motors operate by means of stationary current carrying coils and rotating permanent magnets, therefore the armature remains static which avoids the problem of transferring the current to a rotating armature [5]. In a BLDC, the commutator assembly is replaced by an electronic controller; it uses electronic signal compensation through switching electronics in order to alter the current direction [6]. It undertakes the commutation electronically using rotor position response to determine when to switch the current. Whereas the stator winding works in combination with the rotor permanent magnets in order to produce nearly constant flux density in the air gap which permits the stator coils to be driven by a constant DC voltage which simply switches from one stator coil to another in order to produce AC voltage waveform with a trapezoidal shape. Because of the absence of brushes, it also reduces the maintenance cost.

Outer rotor brushless D.C. motors are especially suitable for applications which require thin motors (short length and big external diameter). Outer rotor brushless D.C. motors have a greater magnet surface, which allows larger air gap and leads to a reduction in mechanical tolerances as compared to inner rotor D.C. motor.

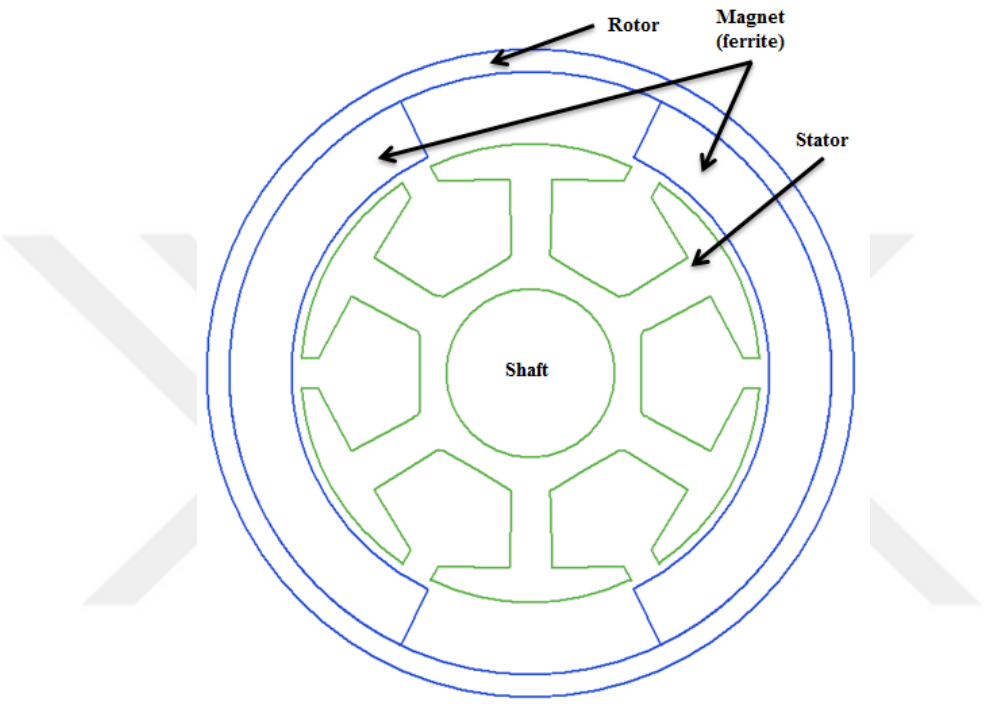

Figure 8: Illustrates the physical configuration of outer rotor BDLC motor.

In outer-rotor BLDC motor the coil windings are confined by an exterior casing comprises of permanent magnets [7]. However, the rotor magnets act as an insulator, which reduce the rate of heat dissipation from the motor. Due to the location of the stator windings, out-spin motor designs typically operate at a lower rated current. The primary advantage of an out-spin rotor BLDC motor is lower cogging torque [8]. The outer rotor configuration is sometimes preferred over the inner rotor configuration and has several advantages in terms of reduced copper losses, reduced production and maintenance cost and required lower energy magnets [7]. When designing an electric motor for an efficient

cooling system, it is important to identify the sources of power losses and to find ways of improving motor efficiency. Motor losses consist of electromagnetic and mechanical losses. However, in order to predict the overall efficiency and total heat dissipated in a motor, the mechanical losses that include bearing losses in outer rotor brushless D.C. motors have to be considered.

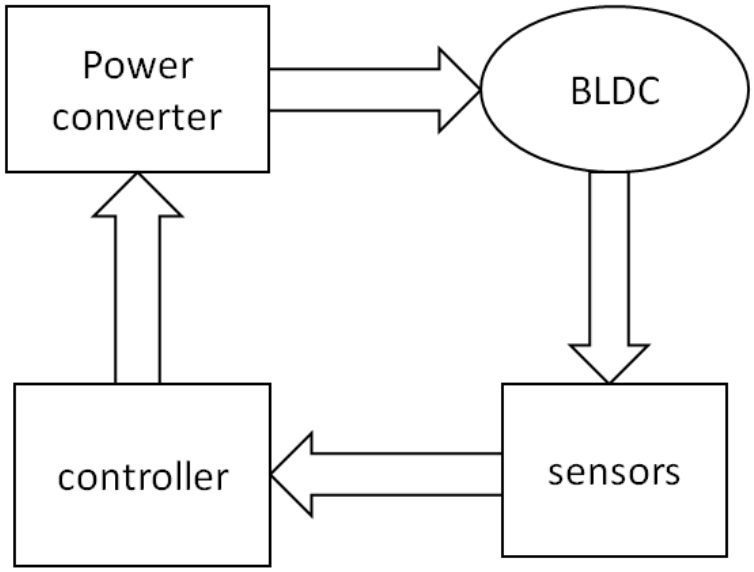

Figure 9: Block diagram of BLDC control.

The main components of a BLDC system power convertor, controller, sensors and motor as shown in block diagram in Figure 9. The power converter is a three phase power semiconductor bridge shown in Figure 10, which convert D.C. power into A.C power so that the motor can transform electrical energy to mechanical energy. The reason for using a sensor in BLDC motor is to determine the position of the rotor, and send it to the controller. The controller requires feedback data about the rotor position so it can generate a pulse width modulation (PWM) duty cycle to power the phases of the

semiconductor bridge. The controller uses a PWM modulator to generate signals that drive the power converter.

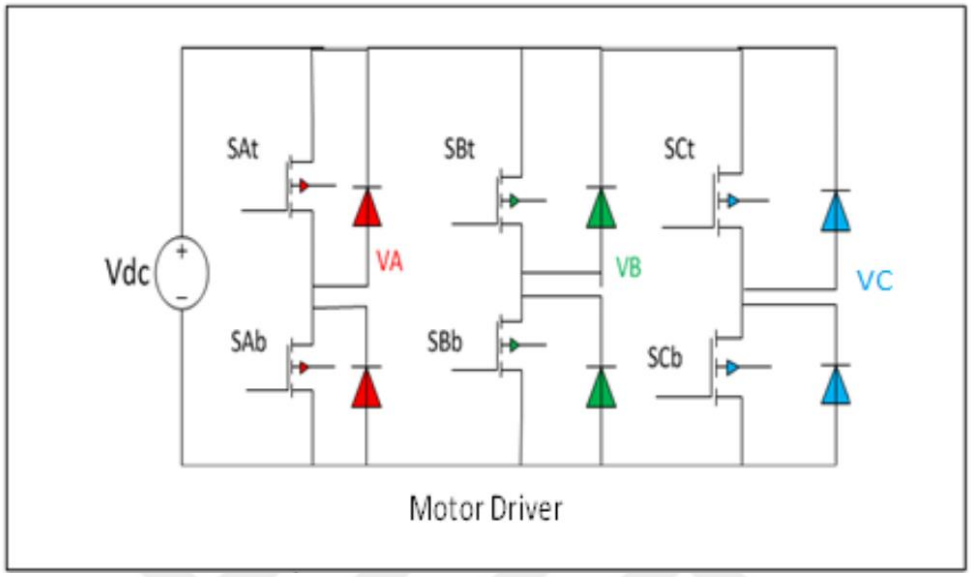

Figure 10: Block diagram of the power converter [9].

Axial Fan Technology

Many investigations have been carried out regarding the axial flow fans and published in the literature during past few decades [10 -11]. An actuator disk model for a low hub-to tip ratio axial fan was established by Thiart and von backstrom (1993). Navier stokes equations were solved by utilizing the k-epsilon turbulence model and the simple algorithm. The fan blades exerted thrust force and torque on the air flow was determined by blade element theory and the effect of partial flow conditions was examined [11]. The empirical correlation developed by Pericleous and Patel (1987) was followed to determine the lift and drag coefficients of blade elements. The method proposed in which the lift and drag forces exerted by the specific element on the flow were further incorporated in the Navier stokes equation as body forces. The increased power associated with the partial

flow conditions was under estimated but good agreement was found with the experiments [12].

The actuator disk model developed by Thiart and von backstrom (1993) was further utilized by Meyer (2000) and Bredell (2005) for the numerical investigation of an air-cooled heat exchanger. At lower flow rates the fan performance was under prediction for the proposed model of Thiart and von backstrom (1993). This can be attributed to the model by taking only the axial and tangential components into consideration in order to determine the relative inflow vector by ignoring the radial component. The radial component of the velocity and the Coriolis effects related with the rotation, become prominent at lower flow rates and induce a delay in boundary layer separation that results in retarded stall.

Van Staden M. (1996) performed a performance characterization of an air cooled condenser by in co-operating the fan performance model into the CFD model. Experimental fan performance curve was utilized to obtain the momentum source term in the axial direction of the fan, which was further added to the Navier Stokes equations as a source term in the CFD model. At an ideal condition, a reasonable agreement was found with the experimental fan performance data, but at non-ideal condition the model required the fan performance curves [13].

Kelecy (2000) performed the performance characterization of a four bladed axial flow propeller over a range of flow rates and comparison made between the data obtained from wind tunnel setup. The blade with the diameter of 0.11 m and has the rotational speed of 2000 rpm was used. The rotating reference frame method of FLUENT was utilized to predict the fan performance by considering a $¼^{th}$ axisymmetric fan model. The flow

equations were solved in the rotating reference frame. The zero velocity was imposed on the blade surfaces and shaft whereas; the outer walls of the model were rotating with the constant speed in the reverse direction with respect to stationary reference frame. The results show the significant pressure gradient were observed at the inlet of the blades at lower flow rates, as the flow rates decreases the radial outflow components from the fan were also observed [14].

Oh, and Kang [15] presented the study regarding the performance characterization of a propeller fan both in axial type characterization at high flow rates as well as radial type characterization at low flow rates. The authors investigated the acute variation in the fans performances at lower flow rates. Around the fan FEA (finite volume method) was utilized to solve the continuity and Navier-Stokes equations in the flow domain. The governing equations used in this study were the continuity and the Reynolds-averaged Navier-Stokes equations for turbulent, viscous and incompressible flow. The fan was placed at the intake of the circular chamber. Reynolds stresses for swirling flow were modeled by using the modified k-ε turbulence model in order to capture the tangential velocity components occurred because of the rotation of the fan. Numerous conclusions were drawn out from the analysis results, where averaged circumferential fluid velocities were used to determine the flow pattern around the fan in radial and axial directions, it was observed that at lower flow rates, the radial velocity components are dominant as compared to axial velocity components around the fan and the fluid around the fan travels in the radial direction. A change in angular momentum occurs between the inlet and outlet of the fan because of the inflow at the hub and outflow at the tip. This change in angular momentum causes rapid rise in static pressure and fan power. At higher flow rates, axial

streamlines flow occurs around the fan region instead of radial streamlines which can be predictable in a normally fan operating condition.

A comparative study of the two fan models MRF (Moving Reference Frame) and lumped fan model has been performed on a specific commercial fan used for electronics cooling by analyzing the flow vectors across the fan axis and by comparing the results with the vendor's data, Shankaran and Dogruoz (2010). Meyer and Kroger [16] simulated the velocity field and overall performance of an axial flow fan by developing an "actuator disk model". The computational results showed a dramatic improvement in predicting the fan performance of an axial fan. However, the model produces errors due to neglecting the radial and tangential forces from the fluid stream and blade tips in the model. Shankaran and Dogruoz (2011) examined the thermal field across the centrifugal blower and axial fan in air-cooled systems by using MRF (Moving Reference Frame) model and lumped fan model techniques. Bleier [2] specified the fan categories according to its application, explained in detail the testing method mentioned in AMCA (Air Movement Control Association) standard and evaluated the relevant applications of fans. Mc Kenzie presented a study related to the design, overall performance prediction, blade loading parameters, flow coefficient diagrams and vortex flow occur across a fan [17]. A similar study has been performed by Liu, Huang and Chen [18], which includes the comparison of the iterative DFR (Downstream Flow Resistance) method with the conventional methods in order to improve the performance prediction accuracy. The inter blade flow field has been investigated and claimed that the dramatic improvement has been observed over the conventional methods.

Corsini and Rispoli [19] simulated the flow physics and predict the overall performance of a non-linear turbulence closure interrelated with high pressure axial ventilation fan. In

this study cubic k-ε turbulence model was employed. A validation test first has been performed on a flat plate with a double circular arc compressor cascade and semi-circular leading edge. The results showed that the improvement in the simulating competences by using a cubic turbulence closure in highly complex flows associated with turbo machinery is obtained. A comparative numerical study performed on the axial ventilation fan, which concluded that the non-linear model shown; provide improved baseline methodology for simulating non-equilibrium effects as compared to the standard model. Whereas the flow visualization at the fan outlet on the tested points, the non-linear solution enhanced the swirl flow prediction and shows reasonable agreement with the LDA data. The refinement of the cubic stress depends on vorticity and strain that reflected to be an acute parameter in modeling 3D flow structure precisely, which is not attainable by using linear eddy diffusivity method.

Linand Huang [20] performed the CFD analysis of a forward curved centrifugal fan and made a comparison in between numerical and experimental results. A CFD analysis was performed by using a commercial CFD Code. The computational domain was splitted into three different regions, inlet region, fan region and outlet region. Different mesh densities assigned to all three regions, according to the intensity and acuteness of the flow conditions. The results used as a tool for adjusting the blade angles and for the diffuser section for low noise levels. Good agreement was found between experimental and numerical results and the error was less than 5.4% for all cases.

Danczyk [21] performed the flow field analysis of an axial fan and compared the results with the tested data. Flow field across the axial fan was analyzed by using the commercial CFD (computational fluid dynamics) code, CFXTASC flow. The CFD model of the fan was generated by using the two rotor blades and three stator blades. The three

dimensional flow fields were investigated around the fan and comparison was made between mid-span values and Laser Doppler Anemometer measurements values obtained experimentally. The boundary conditions were assigned as, at the inlet of the fan total pressure was kept equal to atmospheric pressure and the experimental pressure values were employed at the outlet of the fan. The flow was considered as incompressible and the tip speed of the blades was kept low enough. The computational grid was created in such a way to attain high grid density between the stator blades trailing edge and rotor blades leading edge. The combination of two turbulence models k-ε and k-ω models were utilized for the solution. The reason for using the combination was that k-ε turbulence model under predicts the separation occurs near the walls therefore, k-ω model was utilized close to wall as k-ω model strongly dependent on the free stream flow conditions, the results were excessively sensitive to the inlet specification of ω; therefore, k-ε model was applied at the outer region. The absolute mean velocities showed a reasonable agreement with the flow field values measured values in the free stream areas but the velocity in the wake region was under-predicted. The results for the flow between the rotor blades also showed good understanding but the turbulence level was under-predicted.

Yan and Smith [22] presented numerical study of an axial turbine which comprises of one rotor and two stator rows, and the CFD results were compared with the experimental results. The commercial tool (GAMBIT) was used for constructing a three-dimensional computational unstructured grid and the analysis was done by using a commercial software (FLUENT). The boundary conditions total pressure and static pressure at inlet and outlet were set up according to the experimental results obtained. The periodic sliding interfaces were assigned between rotor and stator boundaries. The turbine blades were

modeled as the rotating blades and the fluid around the blades as rotating fluid. Reynolds stress model was implemented in this study and the flow was considered to be compressible due to high velocities. The results showed exceptional agreement in terms of mass flow rate at the specified conditions, the difference between experimental and numerical results was around 1%. The plane was created at a distance of 8.8 mm of stator blade downstream, Mach number distribution is examined along the plane in the radial direction and it was found 2% higher than experimental results. Mach number distribution showed reasonable results near the mid-span and hub but near the casing Mach number calculated from CFD simulation was slightly higher than the test data. All the results obtained from the CFD analysis were very well predicted with the experimental results. In this numerical study tip clearance of the rotor blades was not considered. However, secondary flows were analyzed by using the unsteady flow calculations whereas, the complex flow details still have not been fully captured.

Ramasubramanian et al. (2008) analyze the fiber diffusion process in the manufacturing of wet-laid nonwovens by incorporating the complete three-dimensional CFD model. The Multiple Reference frame (MRF) was used, the three bladed impeller and baffles were modeled in fluent by using the MIXSIM user interface. Multiple reference frames were used for the impeller which has a diameter of 0.2 m and rotates at 350 rpm, whereas stationary reference frame was used for the baffles and tank. Standard $k-\varepsilon$ turbulence model was utilized for the flow solution. The results were then compared with the experimental work on a mixing tank with baffles and an impeller situated in the center of the tank. The rectangular and triangular effects on dispersion quality were analyzed by the CFD model. The large central vortices produced by the impeller break down effectively by the baffles by reducing the recirculating flow. The model was found beneficial to

predict the source, location and mechanism behind the formation rope and log defects [23].

Paper title	Author	Year Published	Journal/conference	Conclusion
Numerical simulation of the flow field near an axial flow fan operating under distorted inflow conditions	Thiart and backstrom	1993	Journal	- Proposed actuator disk model - Torque and thrust forces exerted by fan blades were determined - Effects of partial flow were examined
Integrated approach to CFD modelling of air cooled condenser	Van staden	1996	Conference	- Perform characterization of air cooled condenser - Obtain fan momentum source term in axial direction - Model was unpredictable at non-ideal conditions
CFD Simulation of an axial flow propeller	Kelecy	2000	Journal	- Perform characterization of four bladed axial propeller - Significant pressure gradients and radial outflow components were observed at lower flow rates
A numerical investigation of dual performance characteristic of small propeller fan using viscous flow	Oh & Kang	1999	Journal	- Perform characterization of propeller fan both in axial at high flow rates and

calculations				in radial at lower flow rates - Radial velocity components were dominant than the axial velocity component at lower flow rates - Angular momentum change occur between fan inlet and outlet due to inflow at hub and outflow at the tip of fan blades Rapid increase in static pressure and fan power due to angular momentum change
Validation of an advanced fan model with multiple reference frame approach	Shankaran & Dogruoz	2010	Conference	- Compared MRF (Multiple Reference Frame) & Lumped fam model - Flow vectors were analyzed across the fan axis
Numerical simulation of the flow field in the vicinity of an axial flow fan	Meyer & Kroger	2001	Journal	- Overall performance of an axial fan by developing actuator disk model - Simulated velocity field across the fan - Results showed dramatic improvement in predicting fan performance - Model produces error due to

				neglecting radial & tangential forces
Advances in fan modeling: issues and effects on thermal design of electronics	Shankaran & Dogruoz	2011	Conference	- Examined thermal field across the centrifugal blower & axial fan in air cooled system - MRF (Multiple Reference Frame) & Lumped fam model techniques were utilized
Fan handbook: selection, application and design	Bleier	1998	Mc. Graw Hill	- Explained in detail testing method of fan mentioned in AMCA (Air Movement Control Association)
Axial flow fans and compressors: aerodynamic design and performance	McKenzie	1997	Ashgate	- Explained in detail about to design, overall performance prediction, blade loading parameter, flow coefficient diagrams & vortex flow across the fan
Performance and inter blade flow of axial flow fans with different blade angles of attack	Liu, Hang & Chen	2011	Journal	- Made comparison in between DFR (Downstream Flow Resistance) method and conventional method - Dramatic performance prediction accuracy was found Inter blade flow field were investigated
Flow analysis in a high pressure axial ventilation fan with a non-linear eddy	Corsini & Rispoli	2004	Journal	- Predict performance of non-linear turbulence closure inter-related with

viscosity closure				high pressure axial ventilation fan - Cubic k-ε turbulence model was used - Non-linear model provide improved baseline methodology for simulating non-equilibrium effects - Non-linear model enhanced the swirl flow prediction
An integrated experimental and numerical study of forward curved centrifugal fan	Lin & Huang	2002	Journal	- Performed CFD analysis of forward curve centrifugal fan - Results were utilized for adjusting blade angles & for diffuser section for low noise levels
CFD simulation of 3-D flow in turbomachinery	Yan & smith	2000	Article	- Presented numerical study of axial turbine - Mach number distribution were examined - Tip clearance of rotor blade neglected in this study - Secondary flow were analyzed by using unsteady flow calculations

				- Complex flow still have not been fully captured
A CFD modelling and experimental study of the mixing process for the dispersion of the synthetic fibers in wet-lay forming	Ramasubramanian, shiffler, Jayachandran	2008	Journal	- Analyze fiber diffusion process in the wet-laid non-woven manufacturing - Rectangular & triangular effect on dispersion quality were analyzed - Large central vortices produced by the impeller break down effectively by baffles by reducing the recirculating flow - Model was found useful to predict the source, location & mechanism behind the formation rope and log defects
The modelling of tangential and axial agitators in chemical reactors	Pericleous & Patel	1987	Journal	- Proposed method to determine lift and drag coefficients of blade element - Increased partial flow power was under estimated in this study
Experimental and computational investigation of the flow field inside an axial fan	Danczyk	2002	Thesis	- Analyze flow field inside of an axial fan - Results comparison was made between laser Doppler anemometer

				measurements and mid-span values - Multiple turbulence models were utilized for the numerical solution - Velocities in the wake region of an axial fan was under predicted
Numerical investigation into aerodynamic blade loading in large axial fans operation under distorted inflow condition	Bredell	2006	Journal	- Utilize actuator disk model proposed by Thiart and Backstorm - Fan performance was under predicted at lower flow rates for the proposed model - Radial velocity components and Coriolis effects were dominant at lower flow rates - Delay in boundary layer separation observed which results in retarted stall

Out-spin Brushless D.C. Motor Technology

Due to the advent of high energy permanent magnets and sophisticated electronic controllers, BLDC motors becomes more popular in a wide range of applications, which include cooling enclosures, machine tools, robotics, aerospace generators, actuators, industrial drives and electric vehicles. Most of the work has been done based on the analytical design approach based on the equivalent circuits model, state space model and lump parameter model [24-25]. Kuria and Hwang present methods for estimating the bearing frictional and electromagnetical losses analytically and numerically for an electric vehicle BLDC motor. The results showed that electromagnetic losses are higher of all losses and also that bearing losses increase assertively with the speed [26]. P. Andrada, M.Torrent, J.I.Perat, B. Blanqué, proposed procedure for computing the power losses in outside spin brushless D.C. motors. Expressions were derived for computing copper losses, power interrupter losses, and stray load losses, stator iron losses in the tooth and in the yoke, mechanical losses, and friction and windage losses. The results were evaluated with the experimental data [27]. Ki-Chan Kim, developed the method for predicting the core losses of the inverter driven BLDC motor by considering pulse width modulation (PWM) of an inverter to regulate the torque or speed of the motor [28]. A study has been performed by S. O. Kwon, J.J.Lee, B. H. Lee , J. H. Kim, ,K.H.Ha and J. P. Hong, related to the power loss distribution in a three-phase induction motor (IM) and a BLDC motor by considering the core material operating point based on the FEA and experimental results. The results showed that in order to improve motor efficiency operating point along with the core materials should be considered [29]. D. L. Gabriel, J. Meyer and F. d. Plessis, presented a method for evaluating and selection of a brushless DC motors (BLDC) used for Unmanned Aerial Vehicles (UAVs) wing [30]. Jinyun Gan presented a

BLDC machine with an exclusive feature of flux regulation and analyze the performance of the motor by using time stepping FEM method [31]. Seung-Chan Park at el performed the analysis of the outer spin rotor BLDC motor takes by considering the effect of eddy current in solid rotor steel shell by using time stepping FEM method [32]. G. H. Jang proposed nonlinear transient finite element analysis of the magnetic field by taking the switching action of pulse width modulation (PWM) into account, which controls the average voltage applied to the motor [33]. Yong Wang performed the transient analysis of an outer-rotor BLDC motor at both normal and flux-weakening operations by using circuit-field-torque coupled transient finite element method. From the above analysis it can be found that by utilizing time stepping FEM technique in machines modeling, the stator current, the load angle, torque and force can be directly computed. Many assumptions such as neglecting material non-linearities, eddy current effect, rotor motion and high order harmonics which are necessary when equivalent circuit model is used, frequency domain FEM model, are no longer necessary. In the BLDC motor, the torque is directly proportional to the winding currents and motor speed which can be controlled by measuring the stator phase voltage applied to the motor [34].

Axial Fan Performance

Axial fans are usually characterized by their performance curves. The curve between the volumetric flow rate and pressure rise dictates the performance of an axial fans. The typical fan performance curve shown below,

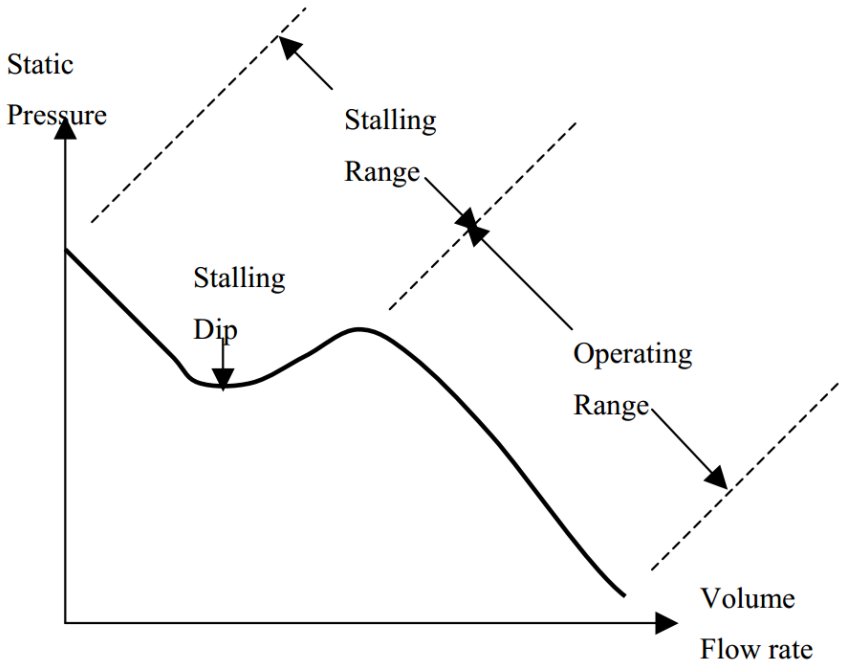

Figure 11: Typical performance curve of an axial fan [2].

The curve starts from the free delivery i.e. the zero resistance at this point the pressure rise value increases to a peak value. As the resistance increases, volume flow rate value decreases, the axial velocity of air also decreases, which responsible for the increase in a lift coefficient and angle of attack and results in the increase of pressure rise. In a typical operating range, axial fan can operate smoothly. In the stalling region, the fan is not capable to operate smoothly; any fluctuation in the static pressure will have an influence on the fan blades as a fluctuating load. At this point, the increase in the flow rate relative to the fan blades causes the static pressure rise and increases the lift force on the blades, the flow is not able to follow the upper contour of the fan blades and therefore, the flow separation occurs on the blade suction side. Flow separation results decrease in lift coefficient and leads to decrease in pressure rise. In the stall region, a small amount of energy coming out from the fan blades is utilize to increase the radial component of the

velocity which increases the static pressure until there is no flow. After this region, the axial flow fan acts in an inefficient and noisy mixed flow fan [2].

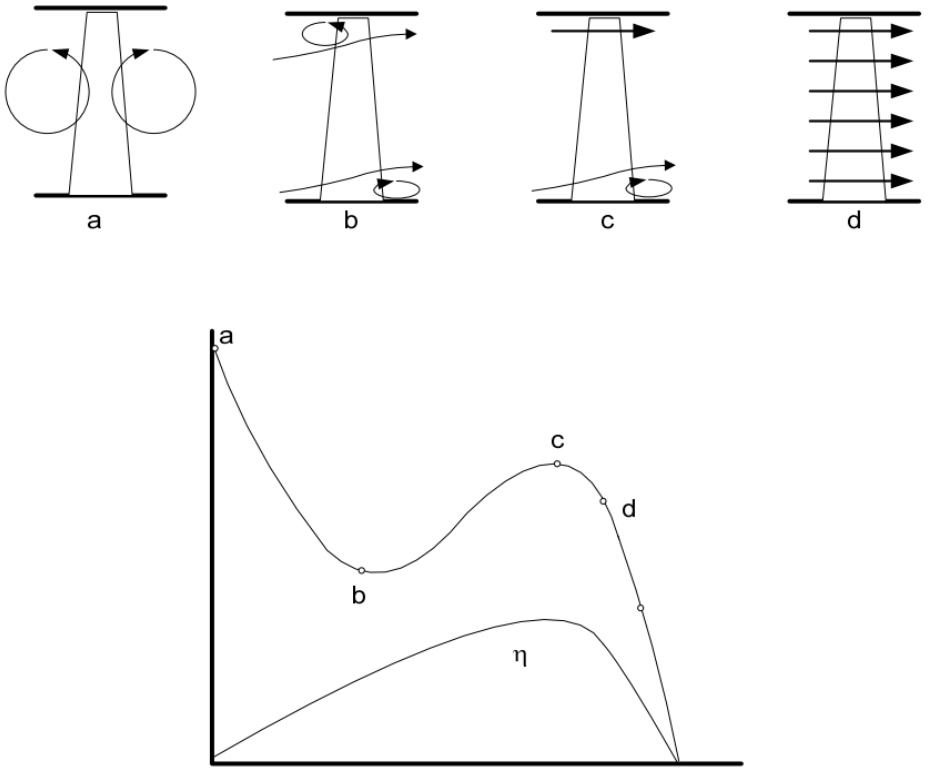

Figure 12: Axial fan performance at different flow conditions [35].

The flow illustration of different points on fan performance curve described in Figure 12. At point “a” almost all of the energy exerted by the fan blades in the form of centrifugal force is utilize to increase the static pressure therefore there is no axial flow at this point. In the region, between points “b” and “c” flow instability occurs at a given static pressure, which results in a rapid change in the volumetric flow rate. At point “d” and so on, the operating range of an axial fan is attained. A good practice for the axial fans is to retain the peak pressure between 30 to 50% greater than the pressure required for the application in order to avoid the fan to operate in noisy and inefficient stalling range. This safety

margin for the pressure will tolerate the inaccuracies which may have been made in the system resistance determination and eliminate fluctuations [2].

Methods for Fan Performance Simulations

It has become a critical to evaluate the fan performance in order to predict the flow distribution and airflow rate for cooling accurately. For the fan performance characterization, the following methods are exists in computational fluid dynamics.

Body force model (BFM):

In this model the fan characteristic is represented as the lumped parameters applied on a fan surface instead of fan blade geometry. The pressure jump and the swirl components are applied as the lumped parameters in terms of flow rate. In most of the cases, only the pressure jump is defined as the fan characteristic. This pressure jump is typically obtained from fan blade curves generated experimentally. Fan characteristic included in this method does not provide an accurate prediction of the flow field but can provide adequate results when computing the flow rate through the fan. The accuracy of body force model is highly dependent on the fan blade curve obtained experimentally [36-37].

Sliding Mesh Model (SMM):

Mostly, rotor stator interactions are time-periodic where the flow cannot be computed exactly using steady state approximation. In order to solve unsteady cases a transient method with sliding meshes can be used. In this method the grid can be divided into different domains connected at the interface that can rotate separately. This method is considered to be the most accurate numerical representation of a rotor stator interaction but it considered to be a time consuming and computationally demanding which makes it impractical for industrial applications [36].

Mixing Plane Model (MPM):

This method averages the properties of the flow circumferentially, which avoids the non-uniformities in the flow field that arises since the fan blades modeled stationary. In this method, the work distance between the rotor (fan blades) and stator cannot be too short. Whereas the errors in the mixing plane increases as the distance between the rotor and stator decreases. Additionally, if the large amount of reverse flow occurs at the interfaces the model will suffer with convergence problem [36].

Multiple Reference Frame (MRF):

The MRF (Multiple Reference Frame) approach also known as the "Frozen Rotor" approach is a steady-state technique and it has recently gained popularity in fan characterization [38-39]. The model simply has two distinct regions, a "fan region" rotating at the same speed as the fan and the fixed region surrounding the fan region. MRF approach does not account for the relative motion of a moving zone with respect to adjacent zones (which may be moving or stationary); i.e. the mesh remains fixed for the computations. The fan zone comprises the actual fan blade, hub and/or finger guard geometry. MRF model does not require any kind of experimental data as an input, as it computes the flow field on the actual fan geometry and its surroundings. While the model is approximate (as it ignores the actual transient features), it can still provide accurate results for many applications [38-39]. While the MRF (multiple reference frame) is an approximate approach, which can provide a realistic model of the time-averaged flow for numerous industrial applications. The MRF model can be utilized for turbo machinery application in which rotor stator interface is comparatively weak. For example, in mixing tanks, where the impeller baffle interfaces are comparatively weak and time stepping effects are not present on large scale, therefore MRF technique can be used. In general,

MRF model can be utilized where transient effects are due to small rotor and stator contact. The MRF model can also be used to analyze the flow fields which can be utilize as an initial condition for a time stepping sliding mesh calculation, which excludes start up calculation requirements [36].

CHAPTER II

MATHEMATICAL MODELING

Governing Equations

For solving the fluid flow motion, the governing equations are continuity, momentum and energy. For incompressible flow, the governing equations for continuity, momentum and energy in tensor notation can be written as follows,

Continuity:

$$\frac{\partial \mathrm{u_i}}{\partial \mathrm{x_i}} = 0 \qquad (1)$$

Momentum:

$$\frac{\partial \rho u_i}{\partial t} + \frac{\partial \rho u_i u_j}{\partial x_i} = -\frac{\partial P}{\partial x_i} + \frac{\partial}{\partial x_j}\left(\mu \frac{\partial \rho u_i}{\partial x_j}\right) \qquad (2)$$

Where, ρ is the density of the fluid, μ is the dynamic viscosity, u is the velocity and P is the pressure.

Turbulence Modeling

For industrial applications, the turbulent flow is widely solved numerically by using the Reynolds decomposition instead of DNS (Direct Numerical Simulation) where the governing equations are solved directly. Whereas in the Reynolds decomposition, the variables are decomposed into a time averaged and a fluctuating component [40].

$$u_i = U_i + u_i' \quad (3)$$

$$p = P + p' \quad (4)$$

After substituting the decomposed term into the continuity and momentum equations for incompressible flow gives the Reynolds averaged Navier-Stokes equations (RANS), above equations can be rearranged and written as,

$$\frac{\partial U_i}{\partial x_i} = 0 \quad (5)$$

$$\rho \frac{\partial U_i}{\partial t} + \rho U_j \frac{\partial U_i}{\partial x_j} + \frac{\partial P}{\partial x_i} - \frac{\partial}{\partial x_j}\left(\mu \frac{\partial u_i}{\partial x_j} - \overline{u_i' u_j'}\right) = 0 \quad (6)$$

Where, the additional term $\overline{u_i' u_j'}$ after decomposing the variables in Navier Stokes equation is termed as Reynold stress tensor. The Boussinesq hypothesis relates the Reynold stress tensor to the mean flow gradients and it can be written as,

$$-\rho\overline{u_i' u_j'} = \mu_t \left(\frac{\overline{\partial u_i'}}{\partial x_j} + \frac{\overline{\partial u_j'}}{\partial x_i}\right) - \frac{2}{3}\rho\delta_{ij}k \quad (7)$$

Where, δ_{ij} represents the Kronecker delta and k is the turbulent kinetic energy which can be defined as,

$$k = \frac{1}{2}\overline{u_i' u_j'} \quad (8)$$

In this particular study, the results are generated by utilizing the realizable $k-\varepsilon$ turbulence model with enhanced wall function instead of standard $k-\varepsilon$ turbulence model. The standard k-ε model may produce non-physical results on or around the solid boundaries; therefore, a modified k-ε model with realizibility constants and low Reynolds corrections was utilized in this study. The term "realizable" indicates that the model

satisfies certain mathematical constraints on the Reynolds stresses, consistent with the physics of turbulent flows. A realizable k-epsilon model varies from the standard k-epsilon model in a way that it can satisfies certain mathematical constraints on the Reynolds stresses, shows consistency with the turbulent flow physics. Furthermore, it can predict the spreading rate of both planar and rounded jets, as well as counter problems concerning boundary layers under strong adverse pressure gradients, flow separation and recirculation more accurately. In the model, the turbulent viscosity (μ_t) was attained by resolving the two transport equations, separated for the turbulent kinetic energy (k) and the turbulent dissipation rate (ε),

$$\mu_t = C_\mu \rho \frac{k^2}{\varepsilon} \tag{9}$$

The two transport equations can be defined as,

$$\frac{\partial k}{\partial t} + U_j \frac{\partial k}{\partial x_j} = \frac{\partial}{\partial x_j}\left[\left(\mu + \frac{\mu_t}{\sigma_k}\right)\frac{\partial k}{\partial x_j}\right] + \mu_t\left(\frac{\partial U_i}{\partial x_j} + \frac{\partial U_j}{\partial x_i}\right)\frac{\partial U_i}{\partial x_j} - \varepsilon \tag{10}$$

$$\frac{\partial \varepsilon}{\partial t} + U_j \frac{\partial \varepsilon}{\partial x_j} = \frac{\partial}{\partial x_j}\left[\left(\mu + \frac{\mu_t}{\sigma_\varepsilon}\right)\frac{\partial \varepsilon}{\partial x_j}\right] + C_{\varepsilon 1}\frac{\varepsilon}{k}\mu_t\left(\frac{\partial U_i}{\partial x_j} + \frac{\partial U_j}{\partial x_i}\right)\frac{\partial U_i}{\partial x_j} - C_{\varepsilon 2}\frac{\varepsilon^2}{k} \tag{11}$$

Where, $\sigma_\varepsilon, \sigma_k, C_{\varepsilon 1}, C_{\varepsilon 2}$ are the empirical constants.

Moving Reference Frame Model

MRF (Moving Reference Frame) is a steady state estimation in which cell zones can rotate/translate individually at different speeds. This approach is suitable for the condition when the flow between the boundary and the zones is nearly uniform which can be achieved by dividing the domain into distinct zones in which flow can be solved in

rotating or stationary coordinate systems. The equations of motion can be written in a rotating reference frame as,

$$\nabla \cdot \overrightarrow{v_r} = 0 \tag{12}$$

$$\frac{\partial}{\partial x}(\rho\overrightarrow{v_r}) + \nabla \cdot (\rho\overrightarrow{v_r}\,\overrightarrow{v_r}) + \rho\,(2\overrightarrow{\omega} \times \overrightarrow{v_r} + \overrightarrow{\omega} \times \overrightarrow{\omega} \times \overrightarrow{v_r}) = -\nabla p + \nabla \cdot \overline{\overline{\tau_r}} + \vec{F} \tag{13}$$

Where, the former and the latter of the last parenthesis on the LHS show the Coriolis and centrifugal acceleration terms respectively. The apparent accelerations in the above equation are the centrifugal acceleration ($\overrightarrow{\omega} \times \overrightarrow{\omega} \times \overrightarrow{v_r}$) which is directed radially outward and the coriolis acceleration ($2\overrightarrow{\omega} \times \overrightarrow{v_r}$) which is directed to the right of the velocity vector. While above two equations are only applicable to the MRF zone, the relationship between the MRF zone and the rest of the computational domain has to be defined. The velocity inside the MRF zone and the velocity in the stationary zone (outside the MRF zone) are written as:

$$\overrightarrow{v_r} = \vec{v} \times \overrightarrow{u_r} \tag{14}$$

Where, $\vec{v}$ is the fluid velocity outisde the MRF zone and $\overrightarrow{u_r}$ is the velocity of the rotating reference frame, which can be written in terms of the rotational speed of the fan zone, $\vec{\omega}$ as follows:

$$\overrightarrow{u_r} = \vec{\omega} \times \vec{r} \tag{15}$$

Where, $\vec{\omega}$ is the angular velocity and $\vec{r}$ is the position vector to the rotating frame.

DC Motor Losses

1.1.1 Electromagnetic losses

Electromagnetic losses in electrical motors are composed of the eddy current loss and the hysteresis loss. Total core loss, which consists eddy-current loss and hysteresis loss in electrical machine, is given in form,

$$P_{core} = K_e f^2 B^2 + K_h f B^2 \quad (W) \tag{16}$$

Where, K_e and K_h are the eddy-current loss and hysteresis loss coefficient, respectively.

Hysteresis loss is revealed when the alternating magnetic field affects the core due to a intermolecular friction. Typical B-H curve of steel core is given below. Area inside the closed curve represents the loss severity whereas eddy-current loss is subdivided into two classes; classical eddy-current loss and excess eddy-current loss. The eddy-current loss occurs because of the conductivity of steel sheets and magnets. The Maxwell equations assumes that when the time and space varying magnetic field intersect with conductive material, the electric field will reveal. Thus, this electric field causes current flowing through the related conductive material either can be steel sheet or magnet. This current causes power loss.

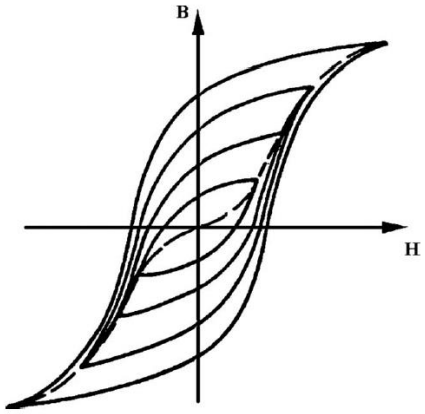

Figure 13: Typical B-H curve.

1.1.2 Inverter loss

The inverter losses are sub-divided into two parts, switch loss P_{sw} and conduction loss $P_{cond.}$:

$$P_{in} = P_{sw} + P_{cond.}\ (W) \tag{17}$$

In switch loss there are two states $P_{sw,on}$ and $P_{sw,off}$. Losses across the inverter can be calculated as:

$$P_{sw,on} = \frac{1}{2} V_{in}\ I_{ph}\ T_{on}\ f_{sw}\ (W) \tag{18}$$

$$P_{sw,off} = \frac{1}{2} V_{in}\ I_{ph}\ T_{off}\ f_{sw}\ (W) \tag{19}$$

$$P_{sw} = n_{sw}\left(P_{sw,on} + P_{sw,off}\right)(W) \tag{20}$$

Where, V_{in} is the input voltage (v), I_{ph} is the phase current (A), T_{on} and T_{off} are switching time (μs), f_{sw} is the operating frequency (Hz) and n_{sw} is the number of switches.

Conduction losses across the inverter can be evaluated by using the following expression:

$$P_{cond.} = \frac{1}{2} n_{sw} I_{ph}^2 \ R_{cond.} \ (W) \quad (21)$$

Where, $R_{cond.}$ represents conductive resistance across the inverter.

1.1.3 Mechanical Losses

In order to accurately predict the overall efficiency and heat generated in a BLDC motor, the mechanical losses, which include friction losses occur between the rotor shaft and bearing, have to be considered [41]. Friction losses occur in bearings can be computed by using the following formula [42]:

$$P_{fr} = \frac{3}{2} n_r \ G_{rot} \ N \times 10^{-3} \ (W) \quad (22)$$

Where, n_r represents the number of bearings, G_{rot} is the rotor weight (N) and N is the speed of the motor (rpm).

1.1.4 Copper losses accounting stray effect

Stray load losses can be defined as the losses that occur due to the non-uniform distribution of a current in copper field. Stray losses result in additional core losses produced in iron due to the distortion of magnetic flux by a load current. Stray load losses can be estimated by using the following empirical expression [43]:

$$P_s = 2 \left(\lambda - \sqrt{\frac{2}{3}} \right) R_{20^0} I^x \ (W) \quad (23)$$

Where, $R_{20}{}^{0}$ is the phase resistance (ohm), $\lambda = \frac{I_{RMS}}{I}$ and usually between 0.86 to 0.84, while exponent *x* can be evaluated and ranging in between 2.8 to 3.6.

D.C. Motor Operation

The function of brushless DC motor is to transforms the electrical input power to a torque on output shaft at a certain angular velocity. Then the fan blades convert the torque and rotational speed into an aerodynamic thrust. Torque of BLDC motor varies due to the back EMF and phase current through the motor winding.

$$T_{mean} = 3\ \frac{E_{ph_{rms}}\ I_{ph_{rms}}}{\omega}\ (N.m) \qquad (24)$$

Where, E_{phrms} is the root mean square value of phase back EMF (v), I_{phrms} is the root mean square value of phase current (A) and ω is the angular velocity of the rotor (radian/sec.).

Kinetic energies of the fluid particles coming out from the fan exit can be estimated by utilizing the following formula [12]:

$$k = \frac{3}{2}\left(u_{avg}\ I\right)^2 \left(\frac{J}{Kg}\right) \qquad (25)$$

$$k = \frac{1}{2}\ m\ u^2\ (J) \qquad (26)$$

Where, *u* is the velocity is the fluid at fan exit and *I* is the turbulence intensity.

The formulation mentioned was utilized to characterize the overall performance of an axial fan and to evaluate the critical components which affect the overall efficiency of the system.

CHAPTER III

NUMERICAL MODELING

CFD Modeling of an Axial Flow Fan

Momentum and pressure fields produced by an axial fan are investigated in this paper. The axial fan of interest is placed in an 82 x 82 x 39 (mm) housing and has two blades with hub and tip radii of 14 and 35 mm, respectively. The nominal voltage and the maximum rotational speed for the fan are 28 V and 19500 RPM, respectively, where the nominal power dissipation is approximately 36 W.

A 3-D CAD model of the fan geometry as shown in Figure 14 is utilized to generate the computational grid. The constructed mesh is illustrated in Figure 15. There are three distinct regions in the computational mesh: through-fan zone, upstream and downstream of the through-fan zone. The former is meshed with hexahedral cells and the latter are meshed with tetrahedral cells.

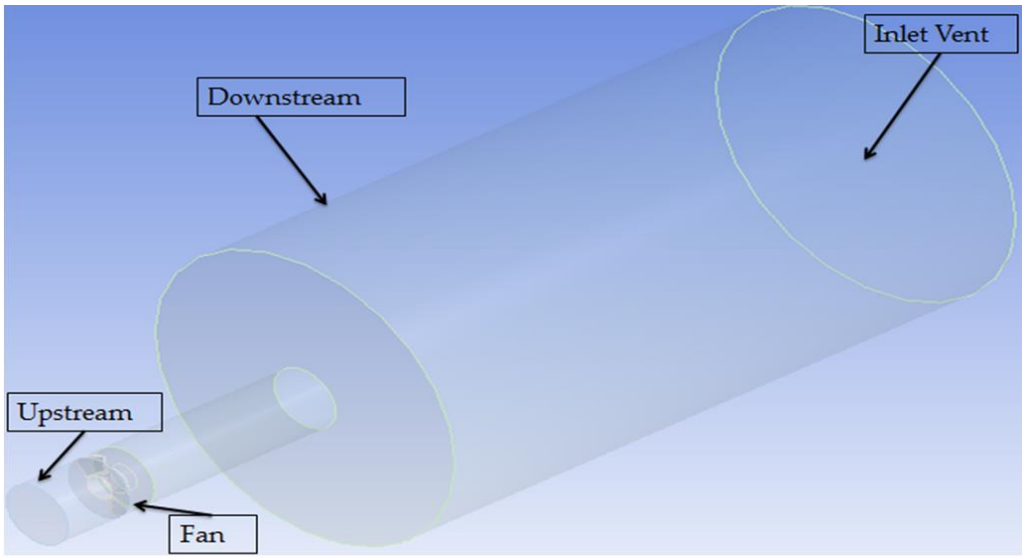

Figure 14: CFD model of the wind tunnel

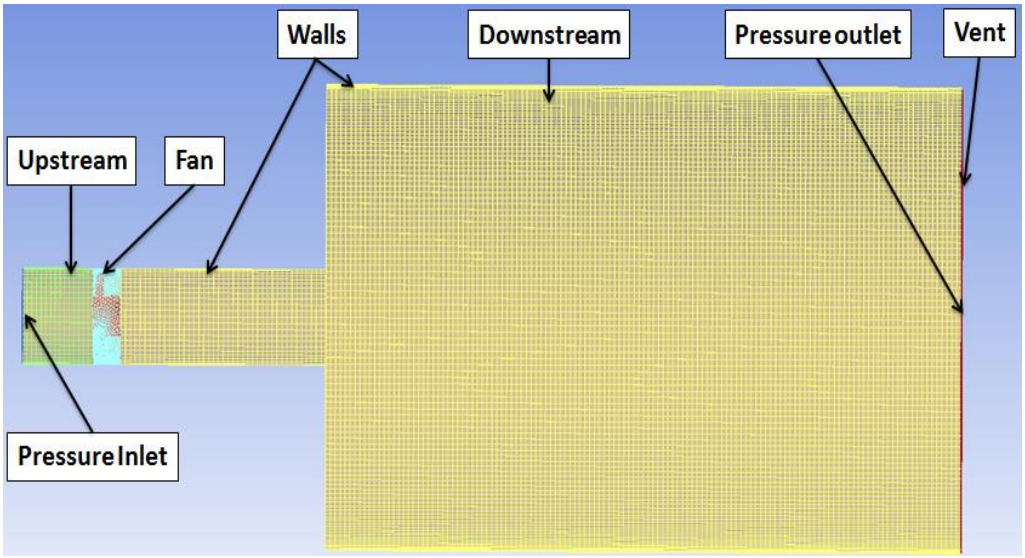

Figure 15. Meshed model with upstream and downstream of the duct.

The mesh characteristic and boundary conditions used for the CFD simulation are summarized in Table 1

Mesh Conditions	**Boundary Conditons**
Hex dominant and prism type mesh	Steady
Number of prism layer : 10	Constant density
First layer thickness (y^+) : 0.213mm	k- epsilon turbulence model
Number of elements : 1.87 million	Pressure Inlet
Number of nodes : 0.9 million	Inlet vent (pressure outlet)
Skewness : 0.93	Three dimensional

Table 1 : Mesh characteristic and boundary conditions.

Hydraulic resistance is varied so that the volumetric flow rate and impedance through the system change. A loss coefficient, K, can be defined to correlate the pressure drop to the exhaust vent to the volumetric flow rate as follows:

$$\Delta P_{vent} = K \frac{\rho \bar{u}^2}{2} \quad (27)$$

Where, ū is the mean velocity right at the upstream of the vent.

A fixed rotational speed of 19500 RPM is applied to the fan (MRF) zone, where the rest of the computational domain is stationary. No-slip boundary conditions are utilized in the wind-tunnel walls.

The results are generated utilizing a realizable k-ε turbulence model. The original k-ε model may produce non-physical results on or around solid boundaries; therefore, a modified k-ε model with realizibility constants and low Reynolds corrections was utilized in this study. The core turbulence model is integrated to the solid boundaries (i.e. the fan hub and the blades) via wall functions where the first cell center is placed in the range of $30 < y+ < 50$. It is hard to satisfy this particular condition for every single cell in the vicinity of the solid boundaries, however an effort is made to keep the first cell center height in this range for the majority of the near-wall cells.

An upwind scheme is used to solve the momentum and turbulence closure equations, where the SIMPLE algorithm is used for pressure-velocity coupling. Convergence is assumed to be reached, when the reduction in total residuals is more than at least three orders of magnitude and the monitor point variables do not vary more than 0.5% for consecutive iterations. All of the simulations are performed with a general purpose CFD tool - ANSYS Fluent 14.5 [42].

Mesh Sensitivity Analysis

A mesh sensitivity analysis is also performed in order to esnure the grid independence. In resolving the flow motion accurately, mesh sensitivity is considered to be a crucial factor

in numerical modelling which depends on the mesh size significantly. Nowadays, the challenge for engineers are dealing with the development of such a model that can satisfy the engineering solutions without considering the fine grid size which will ultimatelty reduce the computational cost. As the grid size gets finer, it imposes a higher computational cost due to the models used as Direct Numerical Simulation (DNS). In contradiction, if the grid size gets coarser, it leads to utilization of the models developed by approximations such as the Reynolds Average Navier- Stokes (RANS), which causes improper depiction of the flow, mainly in case of turbulent flow simulation. Therefore, using the appropriate grid size is always critical. Table 1 summarizes the results showing the pressure rise due to the axial fan as a function of the computational grid size. The pressure rise values are determined to vary less than 1% with the mesh sizes over 1.87 million and therefore the results shown in the next section are generated using this mesh configuration.

Computational Grid Size	Pressure (in.w.g)
6.26E+05	0.498
1.04E+06	0.493
1.55E+06	0.478
1.77E+06	0.466
1.87E+06	0.457
2.06E+06	0.453
2.24E+06	0.454

Table 2: Mesh sensitivity results.

Modeling of an Out-spin BLDC Motor

The power distribution of an inverter driven BLDC motor of an axial fan presented in this study used for electronics cooling enclosures. Figure 16 shows the 2D FEA (Finite Element Analysis) model of BLDC motor. It comprises with the combination of 2 poles and 6 slots. The motor wounded with concentrated winding in order to acheive compact design for the system. The permanent magnet material is ferrite. The inverter creates controllable voltage for speed reference of the rotor by using duty ratio factor.

The core loss distribution of BLDC fan motor is calculated using electromagnetic finite element software ANSYS Maxwell. As it is well known that the flux is not homogenously distributed in core. It is directly related with the magnet positions. The core analysis is performed at no-load condition. Findings are given in the following with response to different mechanical speeds.

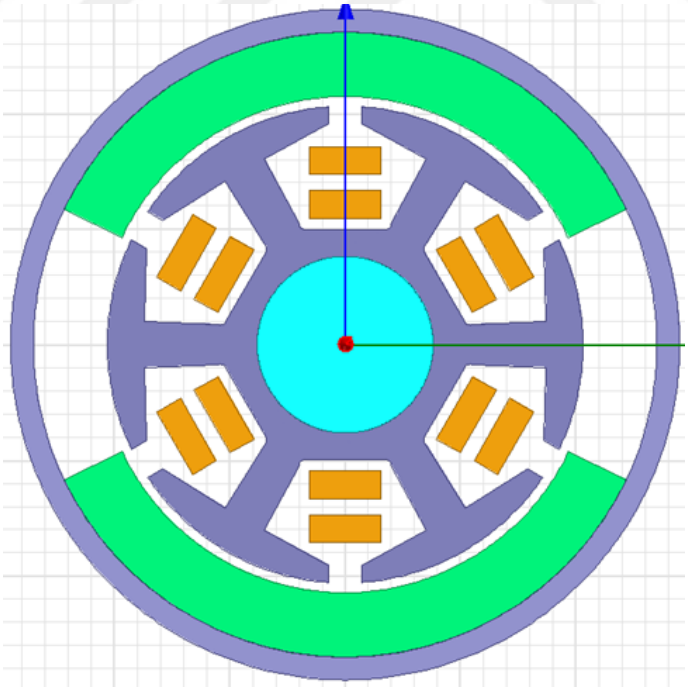

Figure 16. FEA model of outer spin brushless DC motor.

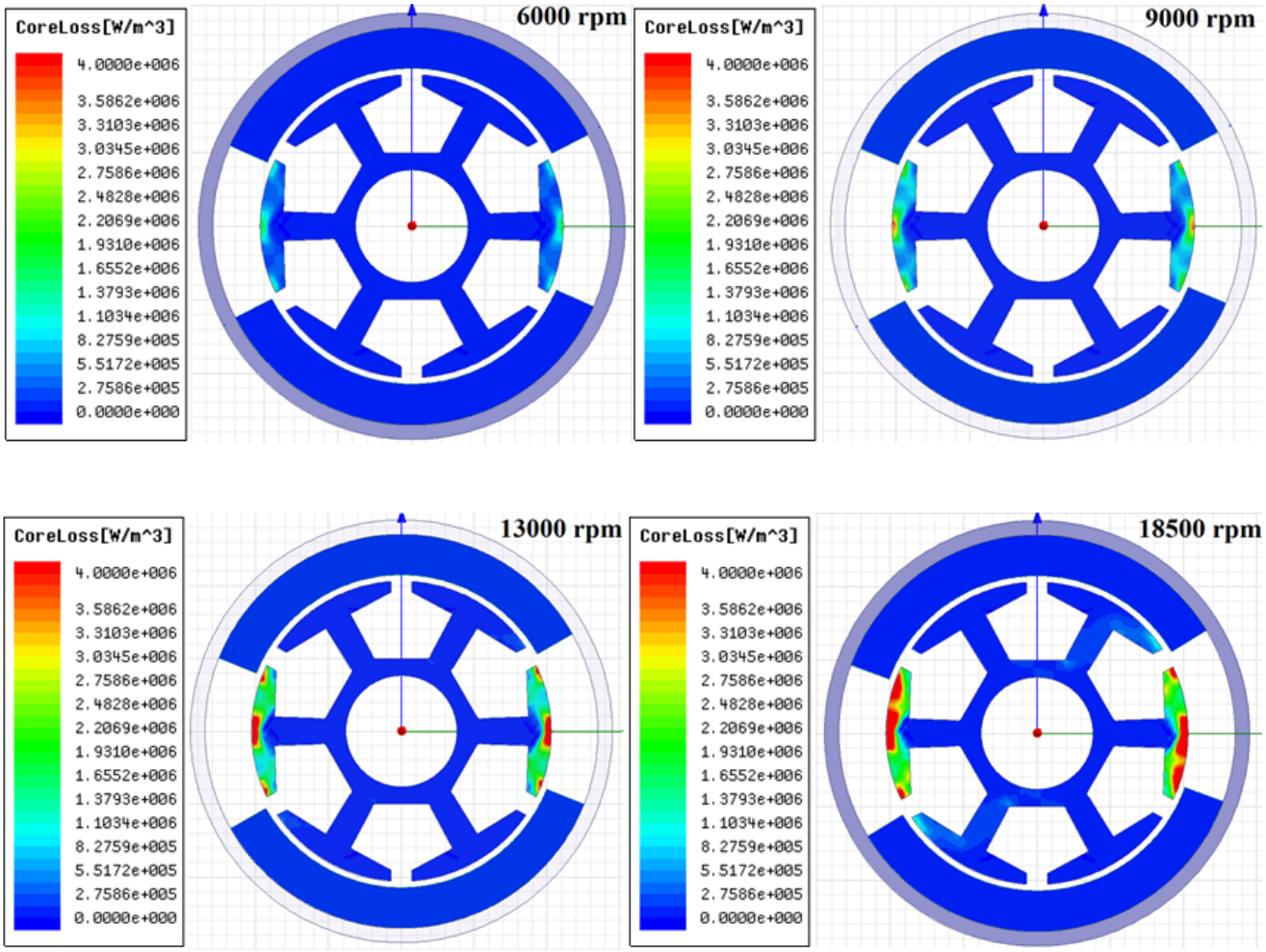

Figure 17: Core loss distribution at different speeds.

The results indicate that core loss value is a function of mechanical speed because the electrical frequency of BLDC motor varies with the mechanical speed. The results verify the electrical frequency core loss relation. Also it can be said that the core loss mainly occurred in stator core. In outer rotor BLDC motor configuration, it is disadvantage because the losses may not be interacted with coolant air flow because of the inlet configuration. Thus the hot spot temperature point of the BLDC will be the stator bore. Figure 17 shows the core loss distribution at different speed at no load condition. As it can be seen that the region of the core loss generation increases with respect to motor speed. Moreover, higher core loss density region are the rotor surface and stator teeth.

CFD Models for Energy Loss Estimation

For estimating the kinetic energy of the fluid particles coming out at the fan exist, CFD (computational fluid dynamics) analysis has been performed. However, energy losses of an axial fan are interrelated to the geometrical losses of an axial fan consisting of casing geometry and blade geometry. A 3D CAD model of the fan geometry is utilized to generate the computational grid as shown in Figure 18.

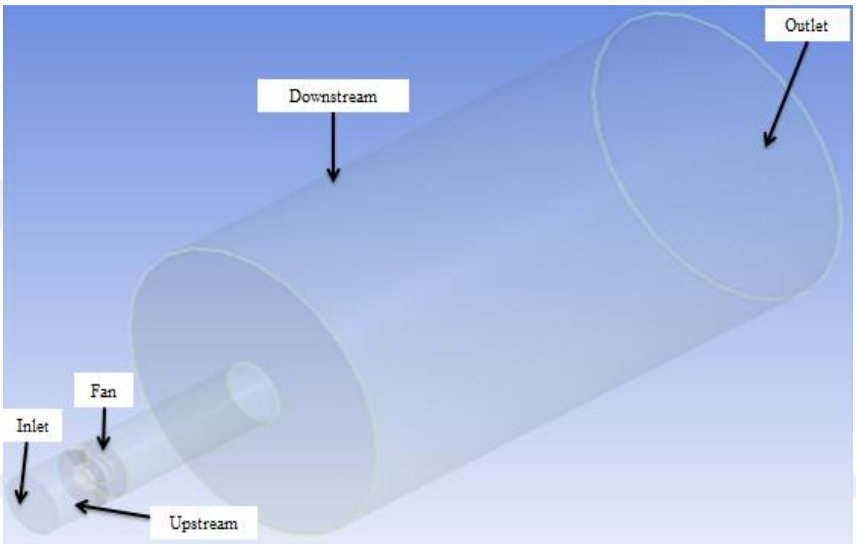

Figure 18: CFD model energy loss estimation.

Figure 18 shows the computational domain of an axial fan test setup consisting of three distinct regions: through-fan zone, upstream and downstream of the through-fan zone. Simulations are performed with a general purpose CFD tool (ANSYS Fluent 14.5). The computational model comprises zero-pressure boundary conditions (P=0) both at the inlet and the outlet of the duct. The analysis is carried out by utilizing the MRF (Moving Reference Frame) technique by running the fan at the nominal speed of 19500 rpm. The plane was created at the fan exit to capture the energy of the fluid particles coming out from the fan rotor. The total energy of the fluid at the fan outlet is comprises of kinetic energy and turbulent kinetic energy which occur due to rotation of the fan rotor.

CHAPTER IV

EXPERIMENTAL STUDY

Wind Tunnel Setup for an Axial Flow Fan

Owing to its multifunctional nature, the axial fans have been widely adopted in various industrial and residential applications. Traditionally, selection of an axial fan is usually concerned with its performance characteristic curve which simply shows the pressure rise against volumetric flow rate. The selection of a particular axial fan design also depends on its application environment as well, i.e. the fan(s) can operate at the intake, exhaust mode or internal to the system.

The apparatus and procedures are prescribed in test codes published by the Air Movement and Control Association (AMCA 210-99) [43]. AMCA provides the methodology for laboratory testing of fans and other air moving devices to determine aerodynamic performance for rating or assurance purposes in terms of airflow rate, pressure, power, air density, speed of rotation, and efficiency. Standard AMCA wind tunnel setup is depicted in Figure 19.

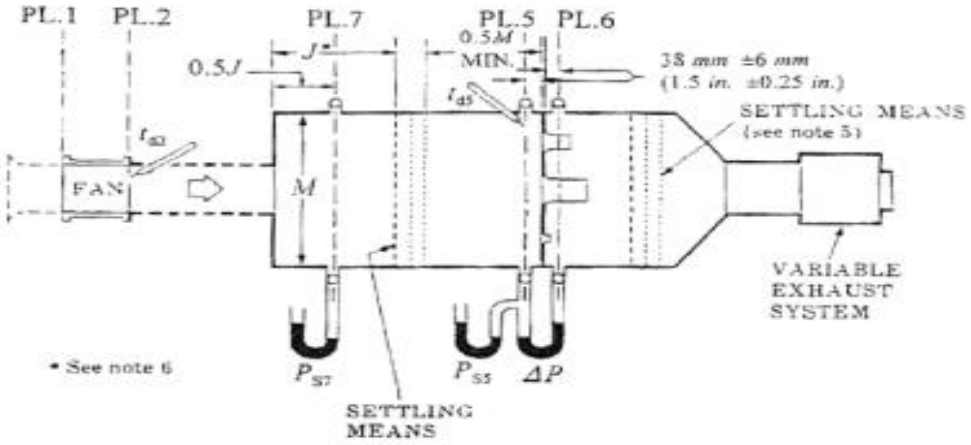

Figure 19: Schematic diagram of wind tunnel setup [43].

The fan testing setup was designed and constructed according to the AMCA standard "AMCA 210-99, 1999" [43]. As shown in Figure 19, a pressure tap attached to an inclined manometer is used to measure the static pressure at the station marked as PL-7. A diaphragm type differential pressure gage is utilized to measure the pressure rise due to the axial fan (i.e. between PL-1 and PL-2) as well as the pressure drop across each nozzle (i.e. between PL-5 and PL-6). As can be seen, the test setup simply consists of a flow straightener (for flow settling), pressure measuring devices and nozzles. However, the pressure drop induced by the flow settling screen is much smaller than that caused by the nozzle; therefore, the screen resistance is actually ignored. The schematics of experimental setup and detailed cross-sectional view of the experimental setup are depicted in Figure 19 and Figure 20, respectively.

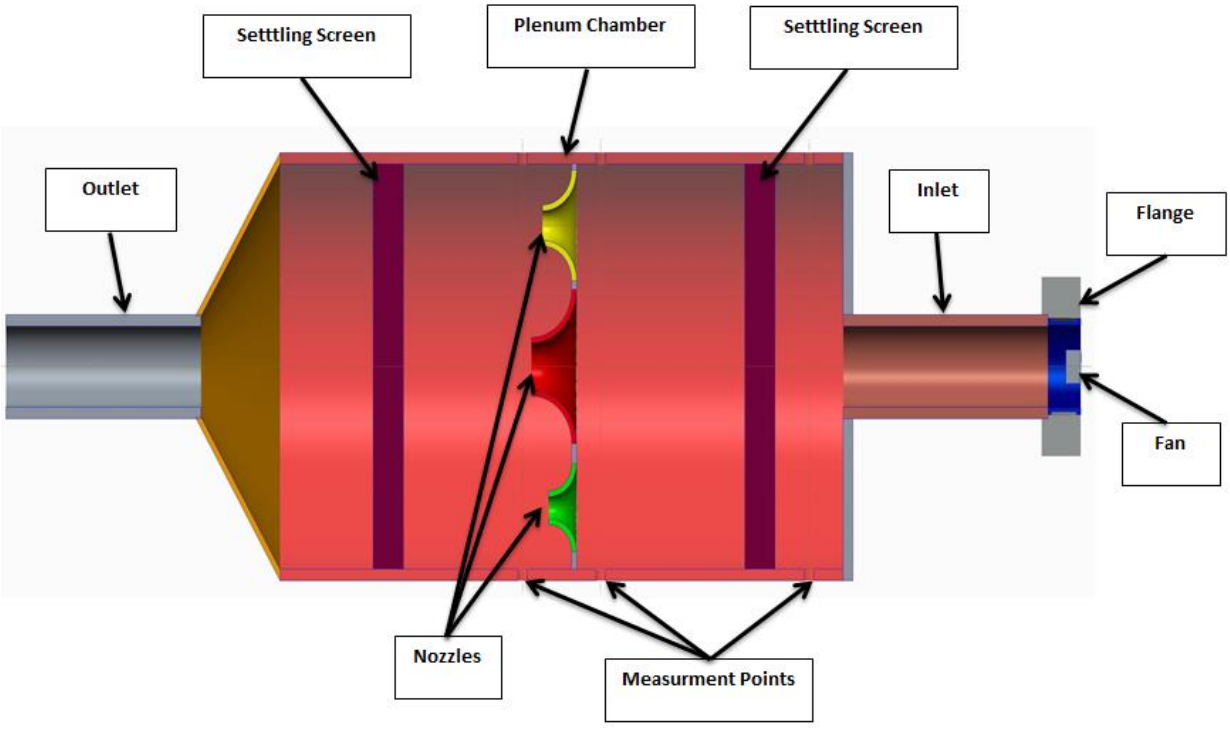

Figure 20: Cross sectional representation of wind tunnel setup

Figure 21: Wind tunnel setup

Figure 21 represents the wind tunnel setup for the axial flow fan. The test facility consists of a circular chamber, which comprises mesh screens (for flow settling), pressure measuring devices, nozzles, and exhaust valve as well as a measurement system. Wind tunnel setup is about 1 m in length with a plenum chamber diameter of 350mm. The inlet and outlet opening of the chamber are of 70 mm in diameter and ~200 mm in length. The primary components of the wind tunnel setup are the nozzle wall, plenums and a blast gate used for adjusting the flow rate.

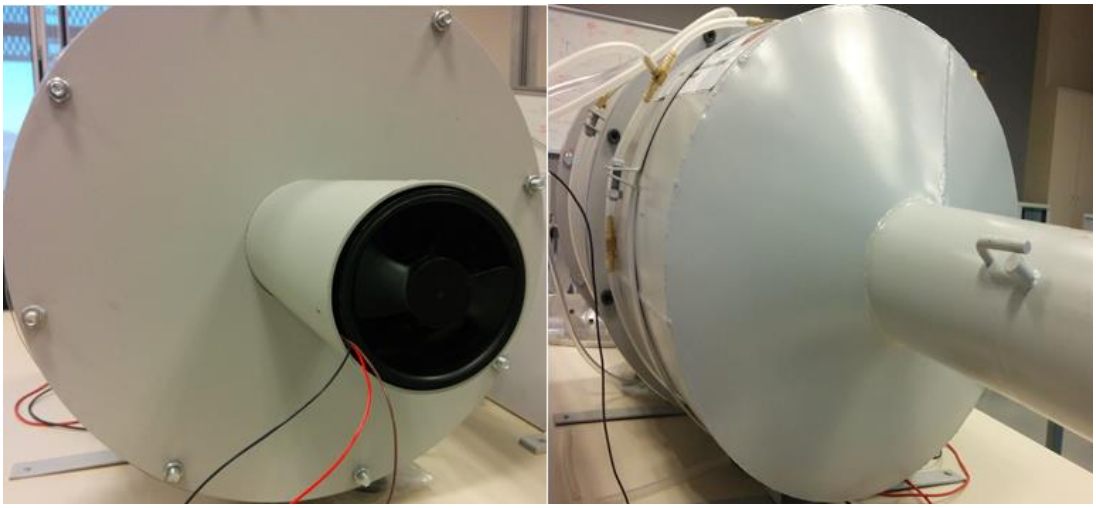

Figure 22: Inlet and outlet of the plenum chamber

The nozzles in the test setup are utilized to measure the volumetric flow rate and are manufactured to the specifications shown by AMCA standard “AMCA 210-99, 1999” [43]. Additionally, each nozzle is only suitable for measurements over a limited range of flow rates shown in Table 3 and several different nozzle sizes may be required to make measurements.

Volume flow rate (CFM)	Nozzle diameter (in.)
24 – 40	0.75 - 1
48 – 71	0.75 - 1.6
63 – 150	0.75 - 1 - 1.6

Table 3: Nozzle selection as a function of flowrate.

Figure 23: Manufactured designed nozzles

A DC power supply is used to operate the fan at its maximum speed by applying the maximum specified voltage without a fan controller. During the testing, the variation in the fan speed is less than 5%. The volumetric flow rate through the system, and therefore

the axial fan, is indirectly determined from the pressure difference due to the nozzles by using the correlations provided by the nozzle manufacturer.

Pressure Measurements

The static pressure in the upstream section of the wind tunnel setup at the station PL-7 is required for the fan curve measurement. For the fan curve measurement pressure at station PL-7 as shown in Figure 19 should be greater than atmospheric pressure. A ring of four pressure taps at the walls of the wind tunnel linked by a mutual tube which is further connected to the inclined manometer (Dwyer, Model 202.5) and with a pressure transducer (Omega, Model PX653-2.5BD5V) are used to measure the average pressure at PL-7. These redundant pressure sensors allow for manual reading and automated data acquisition of the pressure values.

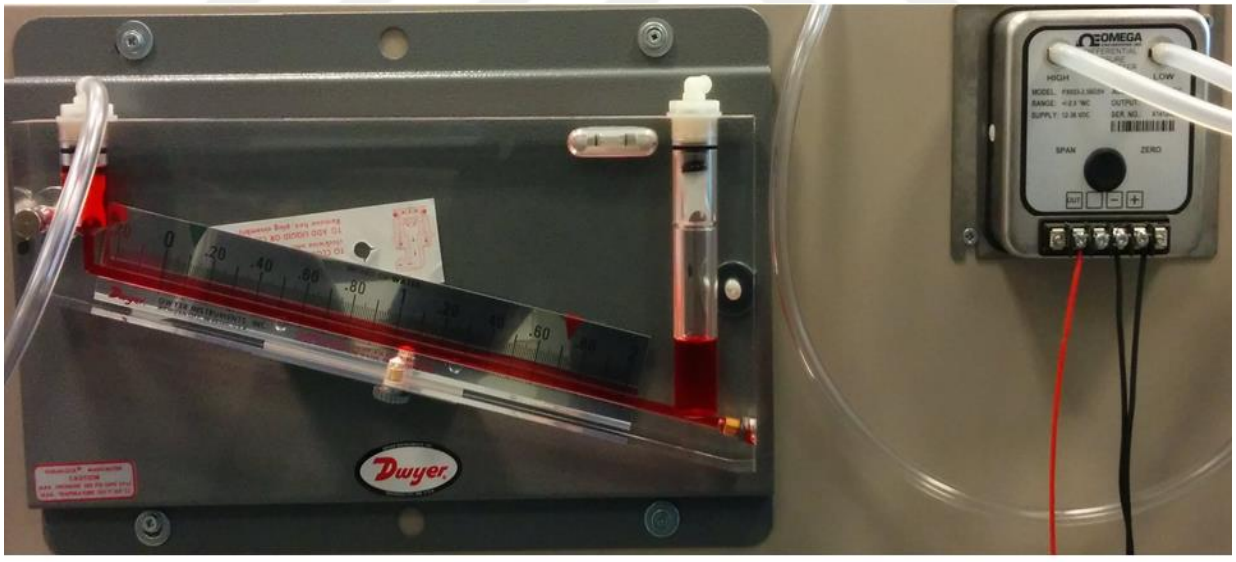

Figure 24: (a) Inclined Manometer (Dwyer, Model 202.5), (b) Capacitance type electronic sensor (PX653-2.5BD5V).

For the pressure drop across the nozzles in order to calculate the flow rate through the nozzle at stations PL-5 and PL-6 as shown in Figure 19, two sets of pressure tap rings (four taps per ring) are used. One set of four taps is situated just upstream of the nozzle wall in the upstream section of the wind tunnel and another set of four taps is located downstream of the nozzle wall in the downstream section of the wind tunnel. The pressure drop across each nozzle is measured by using diaphragm type dial gage (Dwyer Magnehelic, Model 2003C) and with a pressure transducer (Omega, Model PX653-10D5V). From the pressure drop across the flow rate was computed by using the correlation and procedure provided by the AMCA (Air Movement Control Association) standard “AMCA 210-99, 1999”.

Figure 25: (a) Diahragm type dial gage (Dwyer, Model 2003C), (b) Capacitance type electronic sensor (PX653-10BD5V).

Torque Measurements

An attempt for calculating the output torque of BLDC motor through the rotor has been made to study the overall efficiency distribution of the system. A Pulse Width Modulation

(PWM) technique used for the speed measurement in which LED (Light Emitting Diode) and photodiode are used as shown in Figure 26.

Figure 26: (a) LED (SST-50), (b) Photodiode (PDA36A-EC).

The LED (SST-50) from Luminous with a maximum power up to 20W and provides an extremely high output of 1150 lumens from a single chip is used. At the receiver side, photodiode (PDA36A-EC) from Thorlabs is used which is a reverse-biased Positive Intrinsic Negative (PIN) diode coupled with manual switchable trans impedance amplifier (TIA) gain circuit, ranging from 0 dB to 70 dB. The photodiode has an active area of 3.6 mm x 3.6 mm (13 mm2) and a responsivity of 0.1 A/W to 0.5 A/W in the visible light range. The experimental setup shown in Figure 27.

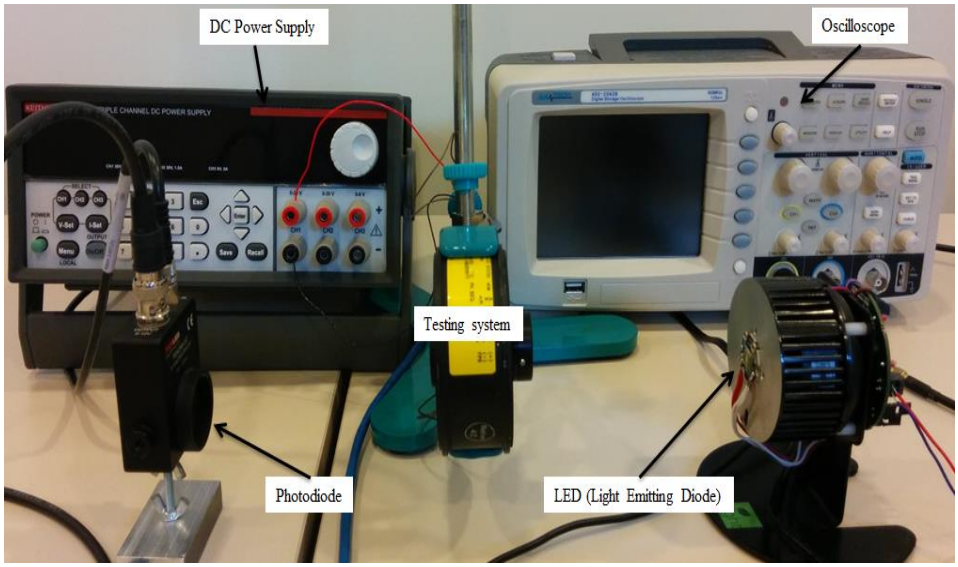

Figure 27: Experimental setup for speed measurements.

Uncertainty Analysis

Uncertainty analysis has been performed to obtain reliable experimental data. It represents the measurable understanding of the errors in well-replicated experimental results.

$$e_g = \left\{(0.01)^2 + \left[0.01\left(\frac{P_m}{P}\right)\right]^2 + \left[0.1\left(\frac{P_v}{P}\right)\right]^2\right\}^{1/2} \quad (28)$$

Where, e_g represents per unit uncertainty in fan pressure, P_m is maximum pressure and P_v is the velocity pressure. Reliability of an experimental study depends on the lower uncertainty. During the early 1950s uncertainty analysis became apparent that various engineering experiments were not repeated enough times in order to deliver statistical data, due to the reason of pressure of time or economy. Therefore, from the last few decades researchers has started given significant attention on uncertainty to get more reliable results. Moffat (1988) mentioned that the experimental data will not be acceptable without the uncertainty analysis involved in the experiments [44]. The usage of the

similar apparatuses over the series of performance at continuous speed usually results in apparently large uncertainties nearly at free delivery and shut off conditions, which are acceptable because performance of the fan is not rated close to these points. Uncertainty analysis is not only crucial in getting reliable experimental data but also essential to figure out the possible cradles of residual error at the first stage of an experiment build-up.

Although, every measurement contains certain amount of error due to that actual value cannot be determined because the error magnitude cannot be known exactly. However, by performing an uncertainty analysis one can identify a range of values within which the actual value lies. A probability of 95% has been chosen as acceptable according to the AMCA standard. The standard deviation of arbitrary inaccuracies can be obtained by statistical analysis of repetitive measurements. An uncertainty analysis is performed and the uncertainty in static pressure (also in volumetric flow rate) measurements is determined to be less than 10%, where it is approximately 2% for the fan power. The uncertainty results are summarized in Table 4**.**

	Pressure (in.w.g.)		
	Nozzle-1	Nozzle-2	Nozzle-3
Minimum value	2.04	1.55	0.70
Maximum value	2.51	1.81	1.30
Relative uncertainty	7.9%	5.7%	9.7%

Table 4: Experimental uncertainty

	Flowrate (CFM)		
	Nozzle-1	Nozzle-2	Nozzle-3
Minimum value	16.7	25.97	44.77
Maximum value	18.6	28.02	61.29
Relative uncertainty	4.42%	3.16%	10.06%

Table 5: Flowrate uncertainty

Torque (mNm)		Relative uncertainty
Minimum value	Maximum value	
2.69	3.14	10.76%
2.91	3.47	12.48%
5.02	4.44	8.65%
5.76	5.89	1.59%
6.97	6.89	0.82%
8.60	7.78	7.14%
9.99	9.73	1.93%
12.58	11.38	7.05%
14.77	15.22	2.11%
17.46	18.38	3.66%

Table 6: Torque uncertainity

Total power loss (W)		Relative uncertainty
Minimum value	Maximum value	
9.59	10.24	4.66%
10.02	10.89	5.87%
10.51	11.40	5.77%
11.22	12.51	7.67%
12.01	13.41	7.74%
12.56	14.44	9.85%
13.71	15.51	8.69%
14.51	17.15	11.80%
16.50	18.79	9.19%
17.70	20.29	9.66%

Table 7: Total power loss uncertainity

CHAPTER V

RESULTS AND DISCUSSIONS

Fan Curve Measurements (Model Validation)

Fan characteristics can be described in form of fan curve. The fan curve is basically a performance curve under a specific set of conditions. In addition, the fan curve depicting the fan performance data of a number of inter-related parameters graphically. Typically, a fan curve can be developed for a given set of conditions, which includes fan volume, static pressure of the system, fan speed, and brake horsepower required to drive the fan under the certain conditions. Fan performance depends on the certain flow characteristics as the air passes over the fan blades that varies for each generic fan type [45].

Prior to investigating the momentum and pressure fields generated by the axial fan, computational results are validated against the relevant experimental data. The experimental data is obtained from wind tunnel testing as described in the previous section. The simulations are carried out as explained previously by applying different values of loss coefficient at the exhaust side of the computational domain. Figure 28 shows the fan curve obtained by the computational models along with the present experimental data as well as the testing data from the fan manufacturer. As it can be seen, a good agreement is obtained between the computed results and the experimental data for the entire span of volumetric flow rate that can be supplied through the fan, i.e. the maximum discrepancy between the experimental and computational results are within 7-12%, which is within the experimental uncertainty and the numerical error.

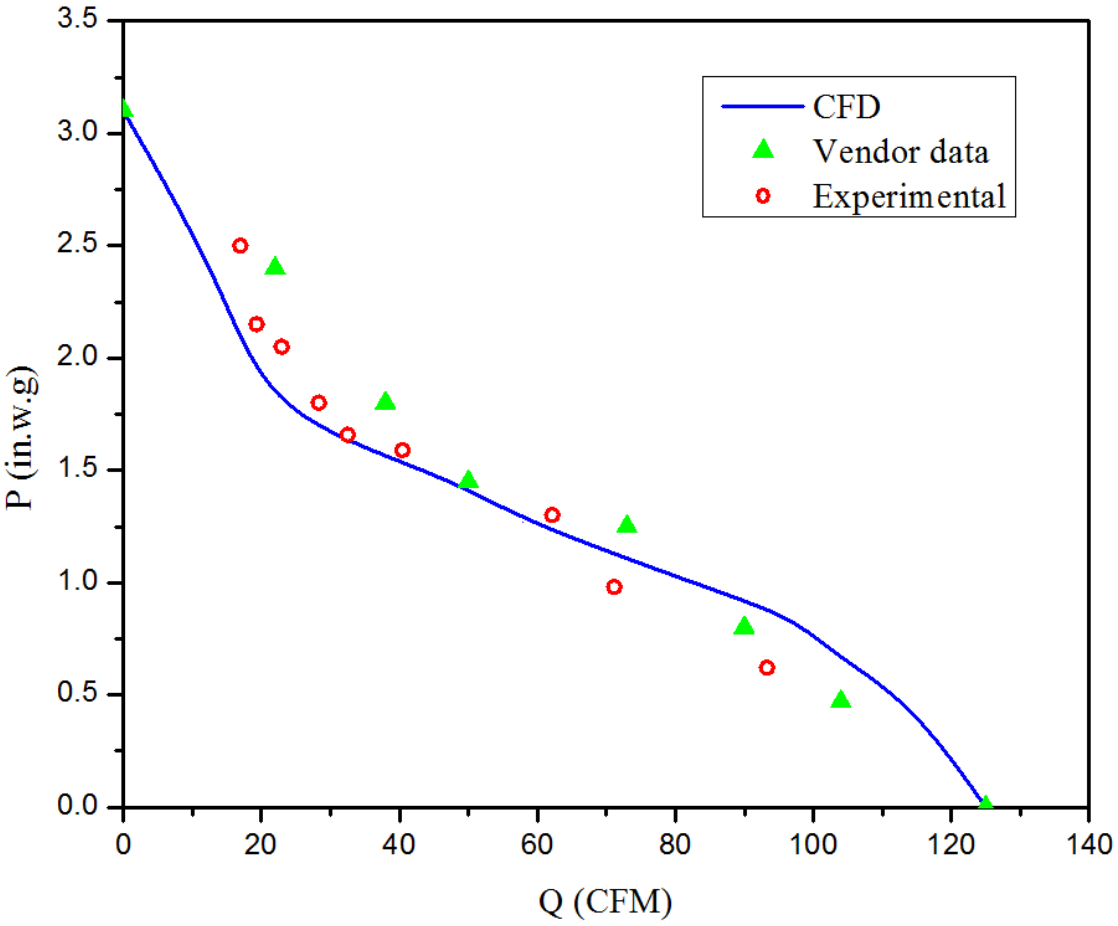

Figure 28: Model validation: Computed P-Q curve (line) against present experimental data (blank symbols) and fan manufactures data (solid points).

Momentum and Pressure Fields

Radial and tangential velocity components produced by an axial fan are comparable with the axial velocity component and lead to some swirl and centrifugal flow spreading. The magnitude of swirl and spreading is dependent on the operating point, i.e. flow rate and the backpressure on the fan. Figure 29 and Figure 30 shows the computed flow field around the axial fan of interest by using the MRF technique. For various loss coefficient values of the vent, K, placed at the exit of the downstream duct, the flow field both to the upstream and downstream of the fan changes significantly. As it can be seen, for the fully

open case (K=0), the recirculation zone behind the fan hub is relatively small and it only extends up to nearly a fan diameter at the downstream of the fan with nearly no disturbance at the upstream. For small values of K, i.e. up to $K \leq 1000$, the height of the recirculation zone is smaller than the fan hub and extends to less than two fan diameters on the fan exhaust side. Nevertheless, if $K > 5000$, both the upstream and the downstream flow fields to the fan show significantly larger recirculation regions. For example, while no upstream. Recirculation zone is obtained at K = 1000, at K = 6250, an upstream recirculation zone is obtained with a height of approximately ($D_f - D_h$).

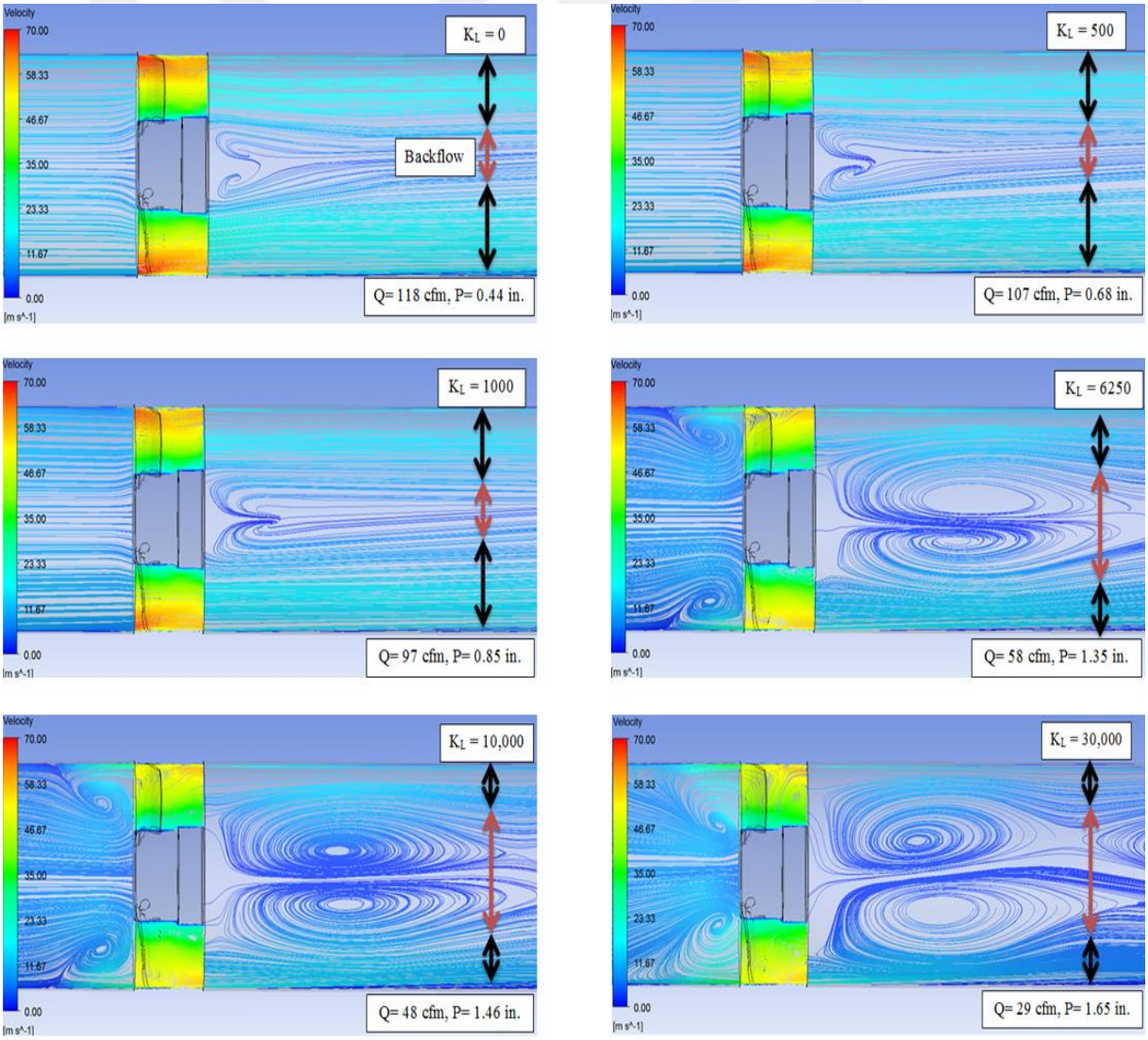

Figure 29: Centrifugal flow distribution for different values of loss coefficient, K.

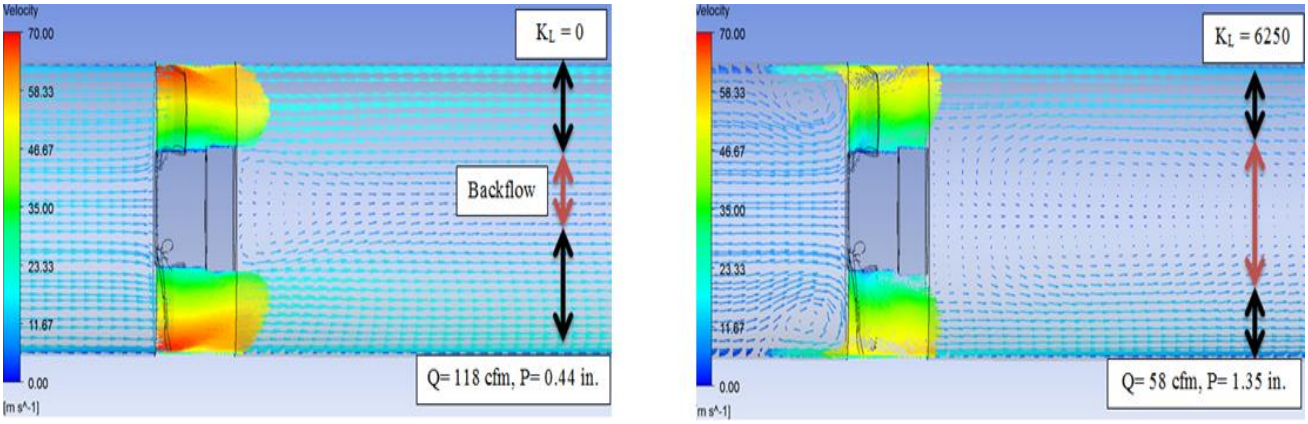

Figure 30: Velocity vectors around the fan for different values of loss coefficient, K.

It is worth noting that the size of the downstream recirculation zone is also significantly larger, i.e. up to three fan diameters at the fan exhaust side. By further increasing the loss coefficient to K = $3x10^4$, the height of the upstream recirculation zone reaches its asymptote of fan diameter, where the downstream recirculation zone extends up to more than four fan diameters downstream of the fan exhaust. It bears noting that for such high impedance systems (large K), the flow field features can no longer be approximated and computed as steady state. As it can be seen, there is a significant asymmetric behavior and the time dependent flow field needs to be computed as transient features dominate. For such cases, transient techniques such as Sliding Mesh (SM) Model can be utilized in computations.

Velocity Field

The velocity field is also examined at a distance of 2.5 fan diameters downstream of the fan exhaust. Figure 31 shows the swirl generated by the axial fan of interest for various loss coefficients on the exhaust vent of the wind tunnel. As it can be seen, at low impedance (low K values), the swirl is more uniform and the flow redistributes more evenly in the cross-section as there is no noticeable recirculation at this axial distance from the fan exhaust (Figure 31). However, with increasing K values, the swirl starts

varying considerably in the radial direction and further increase of K leads to a steep increase of swirl in the radial direction up to distances that are in the near-wall area and vanishes on the wall. While not shown here, at a given K value, the flow field was visualized and it was observed that the swirl became more uniform at further downstream.

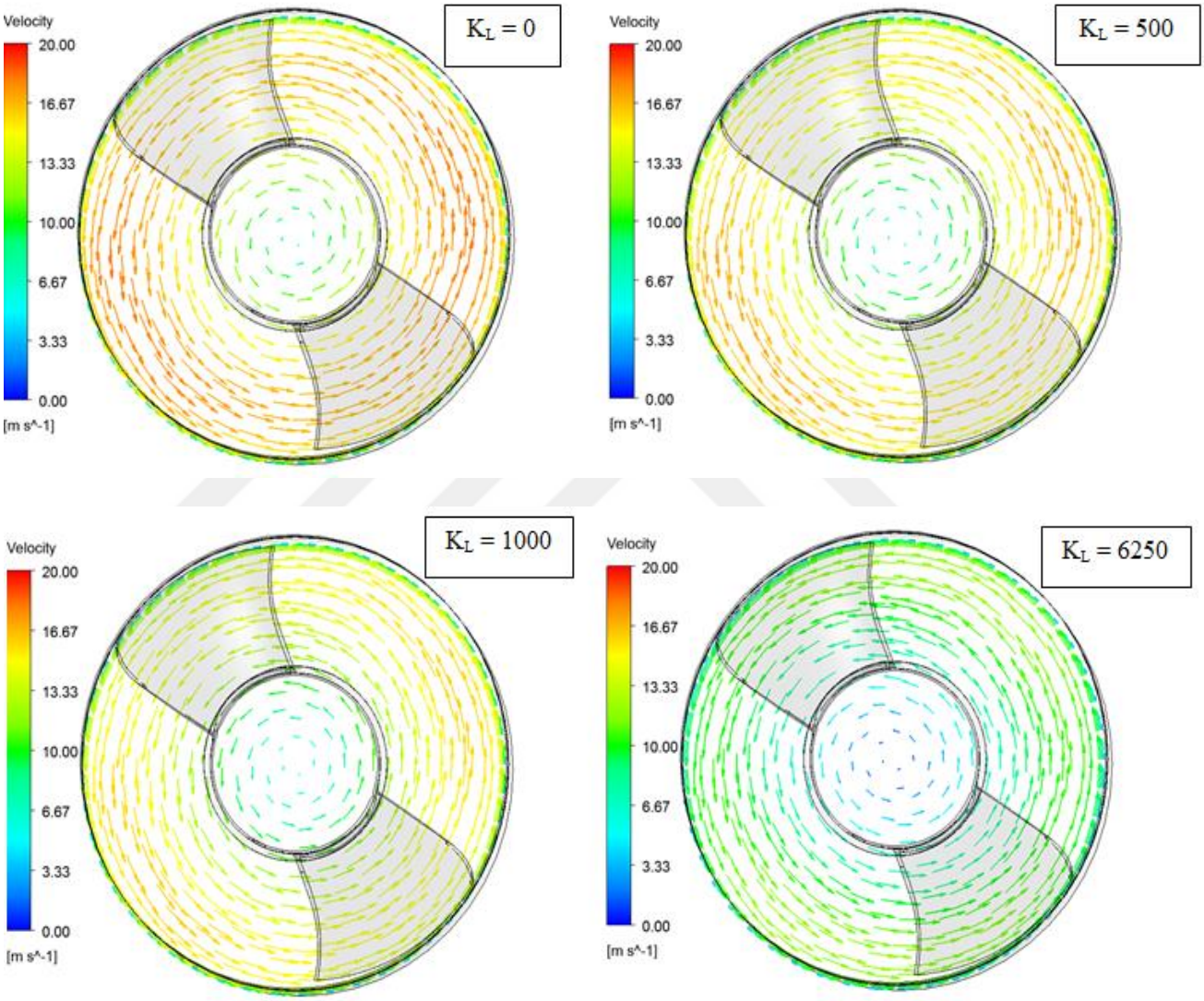

Figure 31: Swirl at the 2.5 outer-fan diameters downstream of the fan for different values of loss coefficient, K.

While not shown here, the flow distribution was also examined by replacing the actual fan model with a hydraulic jump boundary condition which incorporated the experimentally determined fan curve. There was no upstream recirculation zone, and the recirculation region and the maximum velocity at the exhaust side of the fan were significantly smaller than those for its counterpart determined by MRF technique.

Fan Efficiency

Fan efficiency is also determined computationally and compared with the relevant experimental data. The (overall) fan efficiency is defined as the ratio of fan power output to fan power input, where the former is the product of the flow rate and the static pressure rise across the fan and the latter is the product of the voltage drop on the fan and the electric current going through the motor. Therefore, the fan efficiency basically yields null at the two extreme i.e. zero and free delivery points and, in the case of an axial fan the peak efficiency is obtained typically at a volumetric flow rate where $1/3^{rd}$ of the maximum pressure is reached [46]. Therefore, from the fan curve validation results, the peak fan efficiency is expected to occur at $75 < Q < 100$ CFM (where $P < (P_{st} / 3)$, or $P <$ 1.0 in.w.g.). The fan efficiency curve obtained from the computations is shown along with the experimental data in Figure 32. The computational results show that the peak efficiency yields to 27% at a volumetric flow rate of approximately 90 CFM. This is within the range of expectations mentioned above and in good agreement with the experimental data in which the peak efficiency is obtained at a volumetric flow rate range of $65 < Q < 95$ CFM.

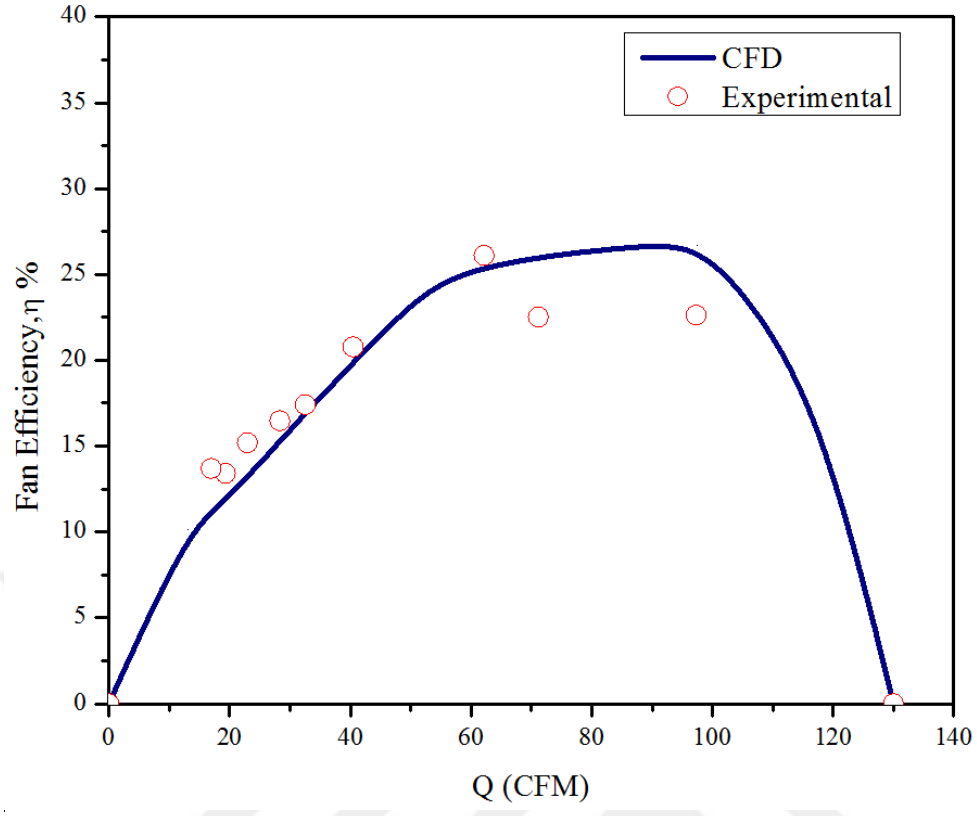

Figure 32: Variation of fan efficiency with the volumetric flow rate for the axial fan

Power Losses and Torque Measurements

Efficiency of the motor is inversely related to the total power loss occur in the motor. When the motor is to operate at high speeds, then the bearing frictional losses cannot be ignored [47]. The core loss depends on the rotor and stator material properties. Whereas the inverter losses comprise of conduction losses and switching losses. There are six switches which can be turned on and off by the PWM (Pulse Width Modulation) sub-controller. Switching losses are related to the operating frequency of the inverter.

Parameter		Specification	Unit
Motor	Nominal power	36	W
	Torque	17.6	mNm
	Nominal speed	19500	rpm
	Phase resistance	0.35	Ohm
Inverter	Switching frequency	50	KHz
	Duty ratio	0.0375	base

Table 8: Specification of inverter driven BLDC motor.

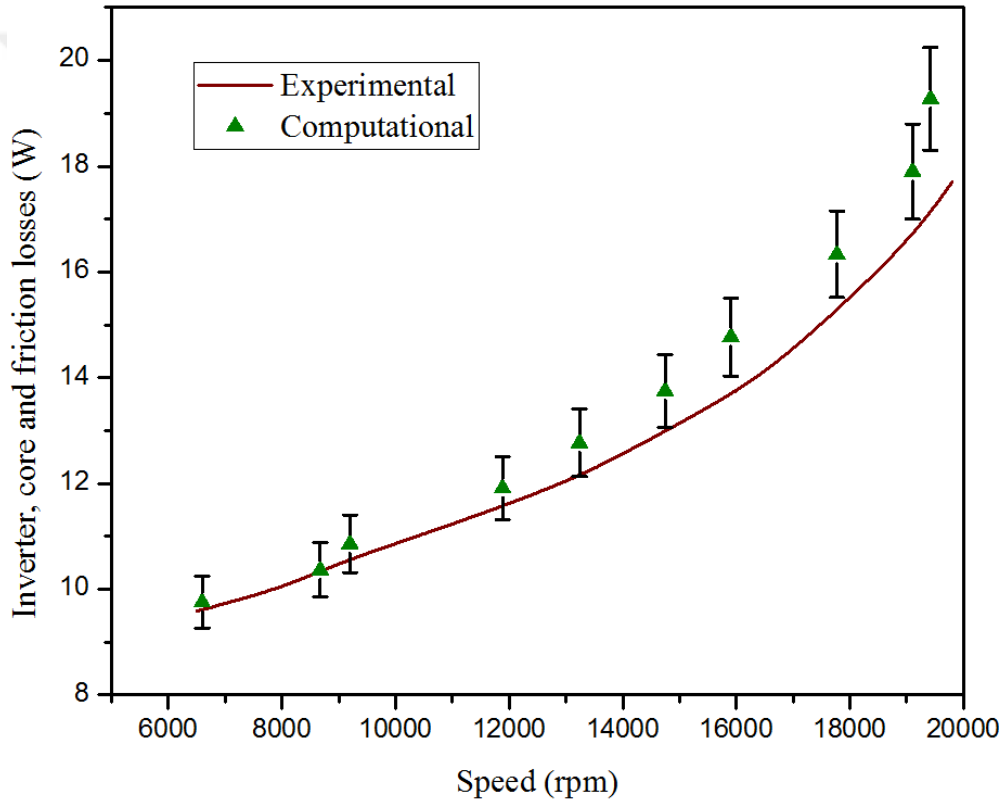

Figure 33: Effect of speed on the inverter, core and frictional losses.

The proposed procedures for evaluating the power losses applied to an existing two-pole out-spin BLDC motor. The computed power losses are compared to the data tested. At different speeds, the electromagnetic, inverter and friction losses are obtained. Figure 33 shows variation of power loss with respect to speed. As the speed of the motor increases power losses increases rapidly. A good agreement found between the analytical and

experimental results with an error of ±8%. Discrepancy between analytical and experimental results at high speed region can be attributed to model inaccuracies of core losses given in equation and harmonics occurring non-sinusoidal nature of the driver current. In fact, model inaccuracy influence core losses whereas harmonics plays more important role in the copper losses.

The torque comparison study has been performed both analytically and experimentally. The losses that depend on the torque and speed of the motor are considered. These losses generally associated with the magnetic non-linearities which results in the rapid increase in the hysteresis, harmonics and eddy current losses than the predicted operating conditions. Figure 34 shows the comparison between the experimental and analytical torque results obtained as a function of motor speed. The results are closely correlated with an error of ±5 %.

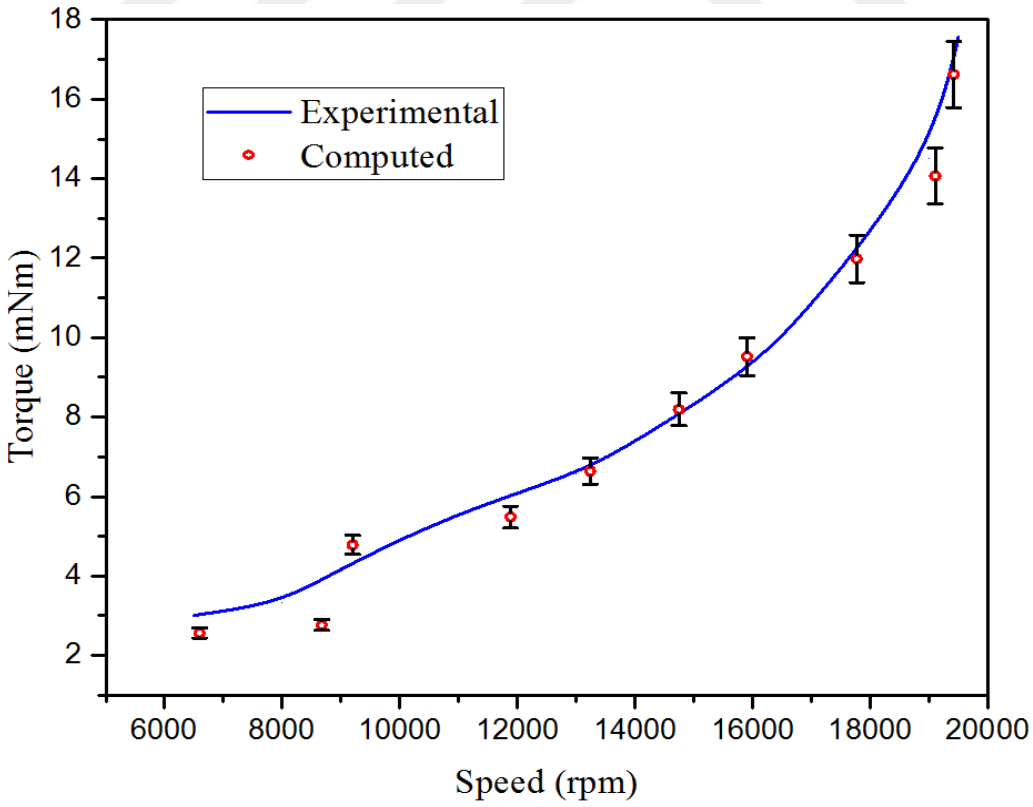

Figure 34: Effect of rotor speed on the total torque.

Overall Power Loss Distribution

As shown earlier, an effort was made to understand the overall fan efficiency as a function of the volumetric flow rate by using the MRF technique. The maximum overall fan efficiency of an axial fan was determined to be less than 27% correlating well with the computational results as depicted in Figure 32. However, the overall efficiency can still be improved; therefore, further investigation into aerodynamic characteristics of the fan blade including leakage and drag losses is required in the optimization of an axial fan system. Fan aerodynamic losses can be subdivided into four major components: tip leakage, profile drag, secondary drag and annulus drag. Tip leakage occurs due to the inherent pressure variation between the pressure and suction side of the fan blade. Reduced tip clearance related flow interactions are necessary in order to improve the energy efficiency of an axial fan and tip leakage is responsible for the significant portion of the energy loss in the axial fan systems. Profile drag is associated with the Reynold number and roughness of the blade; profile drag is considered to be a two-dimensional loss. Reynold number of blade is a function of blade profile and stream turbulence, usually blade Reynold number lies between $2x10^5$ to 10^6 and is directly related to the efficiency where roughness effect can increase the skin friction with a subsequent loss in efficiency. Secondary drag occurs due to the air passage between the blades which depends on the solidity and turning angle of the blade, dissipated in the form of turbulence and heat whereas high skin friction on the boss and wall swept by the blades tips causes annulus drag. The absolute drag acting on the blade varies as the mean relative velocity between the fan blades and the fluid. These losses are a function of velocity pressure which increases with the higher air flows an analysis has been performed in estimating the kinetic energy of the fluid particles at fan exit show that the energy of the

fluid consumed within the system from the power provided by the shaft to the fan blades with respect to input power is about 21%. Energy losses are associated with the tangential component of the velocity imparted by the fan rotor.

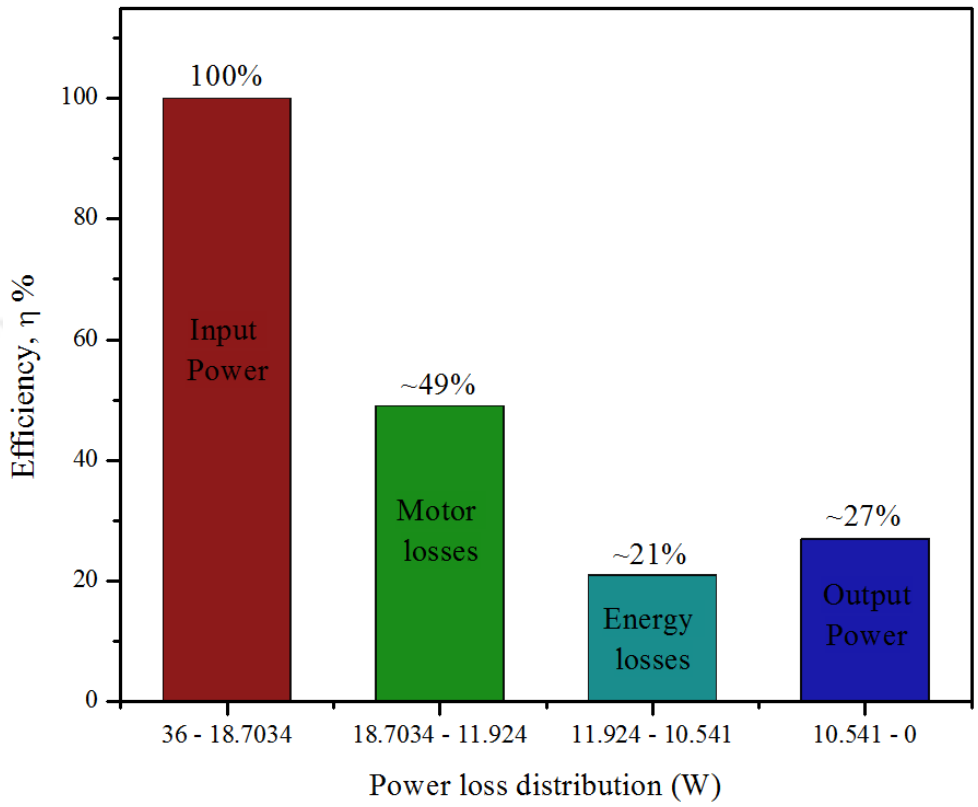

Figure 35: Power losses distribution.

Figure 35 shows the overall power losses distribution of the complete fan system. As can be seen that the major power losses occur in the inverter based BLDC motor of an axial fan which comprises of inverter losses, core losses, and frictional losses and increased heat dissipation also contributes some part of the power loss where motor winding resistance is the main cause of heat generation within the motor. Energy losses occur due to the aerodynamic characteristics (tip leakage, profile drag, secondary drag and annulus drag) of an axial fan which needs to be considered in optimizing the overall fan system. Apart from the above mentioned power losses distribution there are some other losses that are not taken into consideration. For instance, losses in electrical connections, DC power

supply and millimeter. Although this equipment is pretty efficient but it cannot be said that these losses are zero.

CHAPTER VI

PROPOSED FAN BLADE DESIGN

İn axial fan design fundamental length of the blade at any given radii constitute as a blade element whose function is to produce detailed flow deflections. Axial fans can be designed extensively by considering the isolated airfoil technique. However, the general isolated airfoil method was initially derived in relation to aircraft propellers and continued with the low pressure rise axial fans.

The function of an axial fan is to generate a pressure rise. The axial velocity component along the blade radii unchanged if the pressure rise remains stable, then the flow at the fan outlet will follow the free vortex flow. Axial fan blade efficiency is usually characterized by their lift to drag ratios. Fan rotor design is a function of swirl coefficient and flow coefficient respectively, where stator design is a function of the swirl coefficient only. The axial velocity and dynamic pressure based on axial pressure is utilized to non-dimensionalize static pressures and total pressures across the fan.

When manufacturing cost is also critical along with obtaining highest efficiency, cambered plate blade profile of constant thickness twisted from root to tip is generally utilized.

Cambered Plate Airfoil (CP35)

After various trial cambered plate airfoil is considered Because of its versatility, low manufacturing cost and high possible efficiency, cambered fans blades are preferred options when it comes to axial fans. Cambered plate blade airfoil is a constant thickness airfoil and is widely used in axial fans. The computational resources available now which

allow the designer to rapidly design and optimize an airfoil according to a particular application rather than making a selection from an existing families. Java airfoil software was used in designing the airfoil. As the fan transmits power by transforming angular motion into thrust, a pressure variation occur between the forward and the rear surfaces of the airfoil and a fluid flow behind the blade is accelerated. The design parameters for a cambered fan blade are camber angle, camber location, stagger angle, flow angle and various angles of attack. Twisted from root to tip are commonly used for high pressure rise fans. The design criteria of achieving the desirable performance is based on the following factors:

- Volume flow rate required
- Fan diameter, number of blades
- Speed of the fan
- Pressure head rise
- Solidity of blade

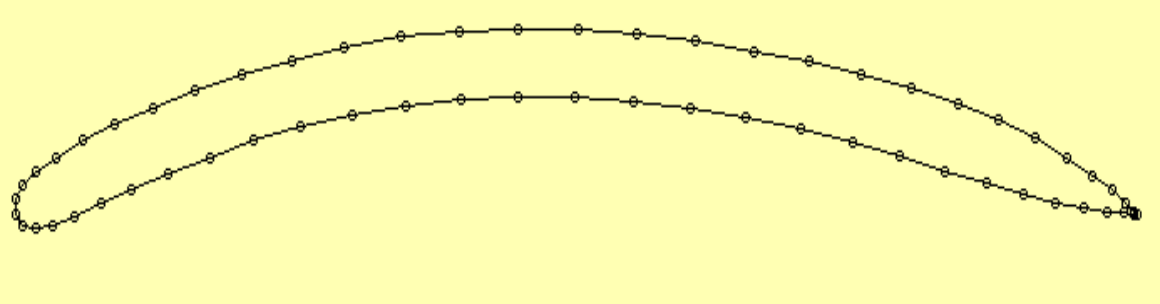

Figure 36: Cambered plate airfoil.

The fan blade was modeled by varying the angle of attack. The calculation for the blade design was done by using commercial EES (Engineering Equation Solver) software. The base parameters that were considered in designing the blade airfoil were volume flowrate, number of blades and rotational speed Characteristic of proposed fan blade (CP35) as shown Table 9.

Parameters	Symbols	Results
Thickness	t/c	4 – 8 %
Camber location	x f/c	45%
Camber	f/c	4 – 10 %
Blade twist angle	θ	18 -35 degree
Aspect ratio	AR	1.673
Span	b	20.5 mm
Axial velocity	V_a	9.315 m/s
Pressure rise coefficient	K_{th}	4.574
Flow coefficient	λ_{MS}	0.3476
Swirl coefficient	ε_{MS}	0.795
Relative inlet flow angle	β_1	70.1 degree
Relative outlet angle	β_2	62.48 degree

Table 9: Specification of CP35.

The CAD modeling was done by commercial CAD software at different angle of attack (α) shown in Figure 37.

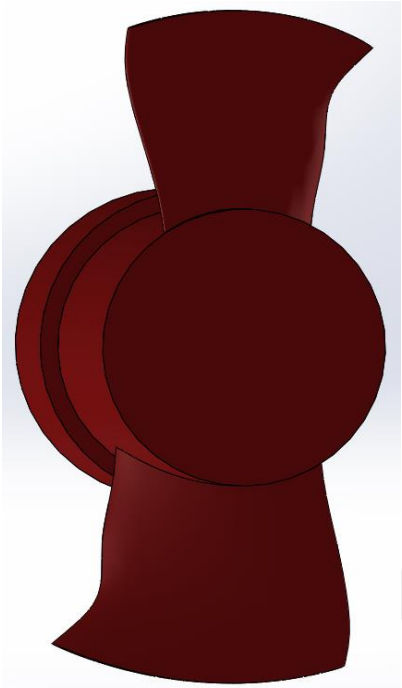

Figure 37 : CP35 CAD model.

In the current design approach the general isolated airfoil method of blade design was adopted, whereas the impeller dynamics can be modeled by using Bernoulli's principle and Newton's third law. Fan efficiency is usually concerned with its characteristic curve. For incompressible flow due to the lower pressure rise, the fan curve of a small axial fan, for standard atmospheric conditions, can be expressed as a pressure difference against volume flow rare at a particular rotational speed. Fan curve for the CP35 fan was obtained numerically by utilizing the DFR (Downstream Flow Resistance) method. The advantage of DFR method is that the back pressure can be adjusted iteratively in order to attain more realistic value during the computational process. Thus, by using the MRF method, primary meshing requirement of the blade airfoil shape can be captured with reasonable accuracy. The simulations were run by applying different values of loss coefficient at the inlet vent boundary condition which is acting as a flow resistance at the exit of the downstream duct. The boundary conditions used in this analysis were pressure inlet and

pressure outlet, as both inlet and outlet pressure were kept at 0 Pa, open to atmosphere. The inlet vent boundary condition was used at the outlet to introduce resistance to the flow. The constant rotational speed of 19500 RPM was applied as an input to the MRF zone, with respect to the stationary reference frame.

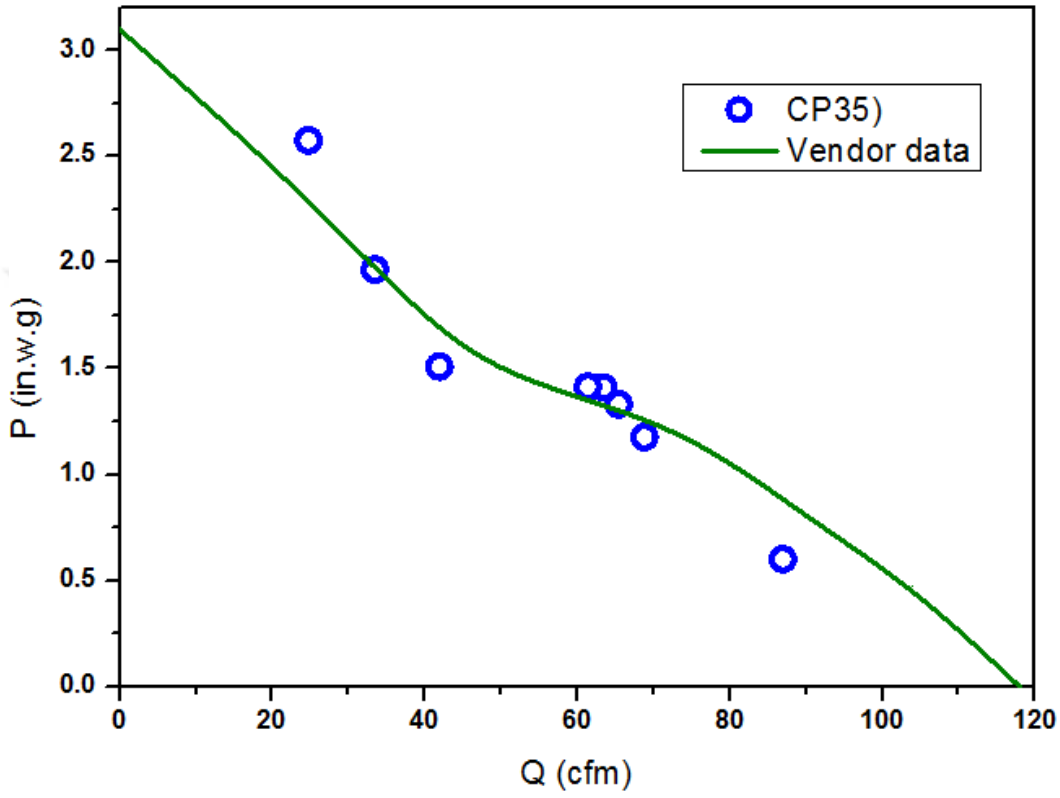

Figure 38. CP35 performance curve comparison.

Figure 38 shows the comparison between the vendors data and CP35 has been made by fan curves. The results show that a further detailed study and an optimization of the blade is required in order to achieve required flowrate and dramatic change in efficiency in the proposed fan blade CP35.

CHAPTER VII

SUMMARY AND CONCLUSIONS

Fan study

Flow field due to an axial fan is investigated numerically and experimentally. CFD computations are performed using the MRF technique. Experiments are carried out following the relevant AMCA test setup and procedures. Fan efficiency is also determined and compared with the corresponding experimental data.

The following conclusions were drawn for the current study:

- Fan operating points computed by the MRF technique correlate well with the present wind tunnel experiments and the vendor's testing data.
- Computations using the MRF model determine that an axial fan with sufficiently far away downstream resistances creates a relatively large size recirculation in the immediate downstream of the fan exhaust and an upstream recirculation region whose size is as large as the fan radius. Higher the system impedance (loss coefficient) is, larger the recirculation zones become.
- Low impedance systems create smaller recirculation zones with more uniform swirl compared to the high impedance systems. Very high system impedance/resistance creates some transient behavior that needs to be resolved using techniques other than MRF.
- For the particular axial fan of interest, the fan efficiency curve determined by computations correlate well with the experimental data, where the peak overall fan efficiency is estimated to be $\eta \approx 27\%$.

Out-spin BLDC Motor

Power losses in inverter driven BLDC motor are investigated by using the procedure proposed and compared with the corresponding tested data. CFD simulation is performed to analyze the core loss distribution as a function of motor speed.

Torque of the motor also determined and compared with the experimental data. The proposed technique is suitable for design studies which require rapid estimation of power losses prior to using finite element analysis. The following conclusions were drawn for the present study:

- The power loss analysis of BLDC motor show that electromagnetic losses are dominant and contribute over 59% of all motor losses, inverter losses contribute around 24%, while frictional losses contribute about 16% of the total power loss.
- In order to attain high motor efficiency, attention must be paid to all sources of power loss in a BLDC motor. However, it is difficult to measure core loss as well as copper loss due to harmonics of voltage and current.
- Characteristics of the motor are affected by inverter parameters such as carrier frequency, duty ratio and frequency of voltage, etc. Moreover, inverter and frictional losses should be included when quantifying motor losses to estimate motor efficiency.
- For the improved overall efficiency of an axial fan geometrical losses should be considered along with the BLDC motor in order to reduce the energy losses across the fan blades and casing.

Future Research

To build a high efficiency axial flow fan for electronic enclosures there are several parameters that need to be optimized in terms of blade design and motor design in order to reduce the energy losses. Based on the conclusion made future research work can be descried as follows.

- In future some mathematical model will be developed for carrying out the performance evaluation of the axial flow fan and the result will be validated form the present experimental results. The optimization of axial air flow fan parameter will be done for the industrial use.
- Blade design optimization and detail study of proposed fan blade (CP35) in order to improve the efficiency and to reduce the energy losses occur across the tip and rotor.
- Performance characterization of inverter driven BLDC motor individually, material properties of winding and magnet for the power loss reduction and with the improved efficiency.
- Cost evaluation will be done for the blade and motor materials in order to reduce overall manufacturing cost, along with the highest possible efficiency.
- Acoustic and noise control study will be performed.
- Assessment of energy consumption with respect to fan performance.

REFERENCES

[1] http://www.rotron.com/fans/index.aspx.

[2] F. P. Bleier, , "Fan Handbook: Selection, Application, and Design," McGraw-Hill, New York, USA, 1998.

[3] T. Kokturk, “Design and Performance Analysis of a Reversible Axial Flow Fan,” The graduate school of natural and allpied sciences, Middle East Technical University, 2005.

[4] T.M. MacRunnel, “Vaneaxial Fan Design and Sizing Using 3D-CAD Modeling Software”, M.S. Thesis, California State University, Long Beach, Department of Mechanical Engineering, May, 1997.

[5] J. R. Hendershot Jr., T. J. E. Miller, Design of Brushless Permanent-Magnet Motors, Magna Physics Publications – Oxford Science Publications, 1994.

[6] A. Emadi, “Handbook of automotive power electronics and motor drives,” A. Emadi, Ed. Florida, United States of America: CRC Press, 2005.

[7] J. Kuria and P. Hwang, “Modeling Power Losses in Electric Vehicle BLDC Motor,” Journal of Energy Technologies and Policy, Vol.1, No.4, ISSN 2224-3232, 2011.

[8] R. Gambhir and A. K. Jha, “Brushless DC Motor: Construction and Applications,” Int. J. Eng. Sci., vol. 2, no. 5, pp. 72–77, 2013.

[8] S. Rambabu, “MODELING AND CONTROL OF A BRUSHLESS DC MOTOR,” M.S. Thesis, National Institute of Technology, Rourkela, 2007.

[10] G. V. Shankaran, M. B. Dogruoz, “Validation of an Advanced Fan Model with Multiple Reference Frame Approach,” Proceedings of the IEEE Intersociety Conference on Thermal and Thermomechanical Phenomena in Electronic Systems, doi 10.1109/ITHERM.2010.5501404, Las Vegas, NV, USA, 2010.

[11] S. A. Beskales, "The Effect of Tip End-blade Geometry On the Axial Fans Performance," Proceedings of the Eleventh International Conference of Fluid Dynamics, ICFD11-EG-4099, Alexandria, Egypt, 2013.

[12] G. Thiart, and T. von backstrom, Numerical simulation of the flow field near an axial flow fan operating under distorted inflow conditions. Journal of wind engineering and industrial aerodynamics, vol. 45, pp. 189-214, 1993.

[13] M. Van staden "Integrated approach to CFD modelling of air cooled condenser", In: 1st south African conference on applied mechanics (SACAM), 1996.

[14] F. Kelecy, "CFD Simulation of an axial flow propeller", Journal Article by Fluent software users, vol. JA108, pp.1-4, 2000.

[15] K.J. Oh, S.H. Kang, “A Numerical Investigation of the Dual Performance Characteristics of a Small Propeller Fan Using Viscous Flow Calculations”, Computers and Fluids, Vol. 28, pp 815-823, 1999.

[16] C. J. Meyer, D. G. Kroger, "Numerical simulation of the flow field in the vicinity of an axial flow fan," International Journal for Numerical Methods in Fluids, 36, pp. 947–969, 2001.

[17] A. B. McKenzie, "Axial Flow Fans and Compressors: Aerodynamic Design and Performance," Ashgate Publ., Aldershot, UK, 1997.

[18] S. H. Liu, R. F. Huang, L. J. Chen, “Performance and Inter-Blade Flow of Axial Flow Fans with Different Blade Angles of Attack,” Journal of the Chinese Institute of Engineers, 34(1), pp. 141-153, 2011.

[19] A. Corsini, F. Rispoli, “Flow Analyses in a High-Pressure Axial Ventilation Fan with a Non-Linear Eddy Viscosity Closure”, International Journal of Heat and Fluid Flow, 2004.

[20] S.C. Lin, C.L. Huang, “An Integrated Experimental and Numerical Study of Forward-Curved Centrifugal Fan”, Experimental Thermal and Fluid Science, Vol.26, pp 421-434, 2002.

[21] S.A. Danczyk, “Experimental and Computational Investigation of the Flow Field Inside an Axial Fan”, Ph. D. Dissertation, Texas A&M University, December 2002.

[22] J. Yan, D.G. Smith, “CFD Simulations of 3-Dimensional Flow in Turbomachinery Applications”, Turbomachinery Flow Prediction VIII ERCOFTAC Workshop, March 2000.

[23] M. Ramasubramanian, D. Shiffler, and A. Jayachandran, "A computational fluid dynamics modeling and experimental study of the mixing process for the dispersion of the synthetic fibers in wet-lay forming", Journal of engineered fibers and fabrics, vol. 3, Issue 1, (2008).

[24] T. W. Nehl, F. A. Fouad, N. A. Demerdash and E. A. Maslowski, “Dynamic simulation of radially oriented permanent magnet electronically operated synchronous machines with parameters obtained from finite element field solutions,” IEEE Trans. Vol.IA-18, no.2, pp.172-181, March/April 1982.

[25] R. Spee and A. Wallace, “Performance characteristics of brushless DC drives,” IAS Annual meeting, pp.1-6, 1987.

[26] W. H. Yeadon, "Handbook of small electric motors", W. H. Yeadon, Ed. United States of America: McGraw-Hill, 2001.

[27] D. L. Gabriel, J. Meyer and F. d. Plessis, “Brushless DC Motor Characterisation and Selection for a Fixed Wing UAV,” IEEE Africon, 2011.

[28] Ki-Chan Kim, “Analysis on Core Loss of Brushless DC Motor Considering Pulse Width Modulation of Inverter,” Journal of Electrical Engineering Technology, Vol. 9, ISSN 2093-7423, 2014.

[29] S. O. Kwon, J.J.Lee, B. H. Lee , J. H. Kim, ,K.H.Ha and J. P. Hong, “Loss Distribution of Three-Phase Induction Motor and BLDC Motor According to Core Materials and Operating,” IEEE Transaction on Magnetics, Vol. 45, N0. 10, 2009.

[30] W. H. Yeadon, “Handbook of small electric motors, W. H. Yeadon,” Ed. United States of America: McGraw-Hill, 2001.

[31] J. Gan, K. T. Chau, Yong Wang, C. C. Chan and J. Z. Jiang, “Design and analysis of a new permanent magnet brushless DC machine,” IEEE Trans. on magnetics, vol.36, no.5, September 2000.

[32] S. Chan Park, B. I. Kwon, H. S. Yoon, S.H. Won and Y.G. Kang, “Analysis of exterior-rotor BLDC motor considering the eddy current effect in the rotor steel shell,” IEEE Trans on magnetics, vol.35, no.3, May 1999.

[33] G. H. Jang, J. H. Chang, D. P. Hong and K. S. Kim, “Finite element analysis of an electromechanical field of a BLDC motor considering speed control and mechanical flexibility,” IEEE Trans on Magnetics, vol.38, no.2, pp.945-948, March 2002.

[34] Y. Wang, K. T. Chau, C. C. Chan and J. Z. Jiang, “Transient analysis of a new outer-rotor permanent magnet brushless DC drive using circuitfield-torque coupled time stepping finite element method,”IEEE Trans. On magnetics, vol.38, no.2, pp.1297-1330, March 2002.

[35] B. Eck, “Fans”, Pergamon Press, 1973.

[36] Fluent 6.2 User’s guide, Fluent Inc., 2005.

[37] A. Wang et al., "Evaluation of the Mutliple Reference Frame (MRF) Model in a Truck Fan Simulation", SAE Technical Paper, Toronto, Canada, 2005.

[38] G. V. Shankaran, M. B. Dogruoz, “Validation of an Advanced Fan Model with Multiple Reference Frame Approach,” Proceedings of the IEEE Intersociety Conference on Thermal and Thermomechanical Phenomena in Electronic Systems, doi 10.1109/ITHERM.2010.5501404, Las Vegas, NV, USA, 2010.

[39] M. B. Dogruoz, G. V. Shankaran, “Advances in Fan Modeling: Issues and Effects on Thermal Design of Electronics,” Proceedings of the ASME International Mechanical Engineering Congress and Exposition, doi 10.1115/IMECE2012-89857, Houston, TX, USA, 2012.

[40] J.H.Ferziger, M. Peric, "computational methods for fluid dynamics", 3rd edition, springer Verlag, Berlin, Germany, ISBN 3-540-42074-6, 2002.

[41] P. Andrada, M.Torrent, J.I.Perat, B. Blanqué, “Power Losses in Outside-Spin Brushless D.C. Motors,”

[42] Fluent 14.5, 2012, User Guide, Ansys Inc., Canonsburg, PA.

[43] ANSI/AMCA Standard 210-99 | ANSI/ASHRAE 51-1999, "Laboratory Methods of Testing Fans for Certified Aerodynamic Performance Rating,” AMCA International Inc, 1999.

[44] R. J. Moffat, “Describing the uncertainties in experimental results,” Experimental Thermal and Fluid Science, vol. 1, no. 1, pp. 3–17, Jan. 1988.

[45] Electrical Energy Equipment "Fans and Blowers" Energy Efficiency Guide ofr Industry in Asia, www.energyefficiencyasia.org., UNEP, 2006.

[46] "Fan Efficiency − An Increasingly Important Selection Criteria," http://www.nmbtc.com/fans/white-apers/fan_efficiency_important_selection_criteria/

[47] D. G. Dorell,” Combined Thermal and Electromagnetic Analysis of Permanent-Magnet and Induction Machines to Aid Calculation”, IEEE Transactions on Industry Applications, vol. 55, no. 10, pp. 3566-3574, 2008.

[48] Air Movement and Control Association. Laboratory Methods of Testing Fans for Aerodynamic Performance Rating, ANSI/AMCA Standard 210-99. Air Movement and Control Association International, Inc., Arlington Heights, IL, 2000.

[49] R. A. Wallis, "Axial Flow Fans, Design and Practice," Academic Press Inc., New York, USA, 1961.

Appendix A

Volume Flow Rate Calculations

The flow rate through the wind tunnel is measured by the throat radius of flow nozzles which was built according to the specifications described in AMCA standard 210-99. The volumetric flow rate (Q) through the nozzle can be calculated as

$$Q = C_d\, Y\, A_n \sqrt{\frac{2\Delta p}{\rho(1 - \beta^4)}}\ (CFM)$$

Where, C_d is the nozzle discharge coefficient, Y is the expansion factor, A_n is the nozzle throat area (m2), Δp is the pressure drop measured across the nozzle (Pa), ρ is the fluid density (Kg/m^3) and β is the contraction ratio.

The expansion factor can be calculated as [47],

$$Y = \sqrt{\left[\frac{\gamma}{\gamma - 1}\gamma^{2/\gamma}\ \frac{1 - \alpha^{(\gamma-1)/\gamma}}{1 - \alpha}\right]\left[\frac{1 - \beta^4}{1 - \beta^4\alpha^{2/\gamma}}\right]}$$

Where, γ is the specific heat ratio (for air γ= 1.4) and α is the ratio of the nozzle exit pressure to upstream nozzle pressure is represented as,

$$\alpha = \frac{p - \Delta p}{p}$$

Where, p is the upstream pressure (Pa).

Whereas, nozzle throat area (A_n) and contraction ratio (β) can be calculated as,

$$A_n = \frac{\pi d_t^2}{4}$$

$$\beta = \frac{d_t}{D}$$

Where, d_t and D are the throat diameter (m), upstream diameter (m) respectively.

For the nozzle discharge coefficient (C_d), the equation relating C_d and Re_t represented as follows [47],

$$C_d = 0.9986 - \frac{7.006}{\sqrt{Re_t}} + \frac{134.6}{Re_t}$$

Where, Re_t is nozzle throat Reynold number,

$$Re_t = \frac{4Q}{\rho \pi d_t \mu}$$

Where, Q is the volumetric flow rate (m3/s) and μ is the fluid viscosity.

For the calculation of Reynold number, value of Q is required. Therefore, it involves the following iterative procedure,

For measured pressure drop value across the nozzle compute,

$$K_Q = A_n \sqrt{\frac{2\Delta p}{\rho(1 - \beta^4)}}$$

Assume the value of nozzle discharge coefficient (C_d= 0.9) and calculate the volume flow rate by using the following relation

$$Q = C_d K_Q$$

After that compute throat Reynold number (Re_t) then nozzle discharge coefficient (C_d) and compare the value with the assumed value if its close enough then calculate the required volumetric flow rate.

Appendix B

Pressure Transducer Conversion

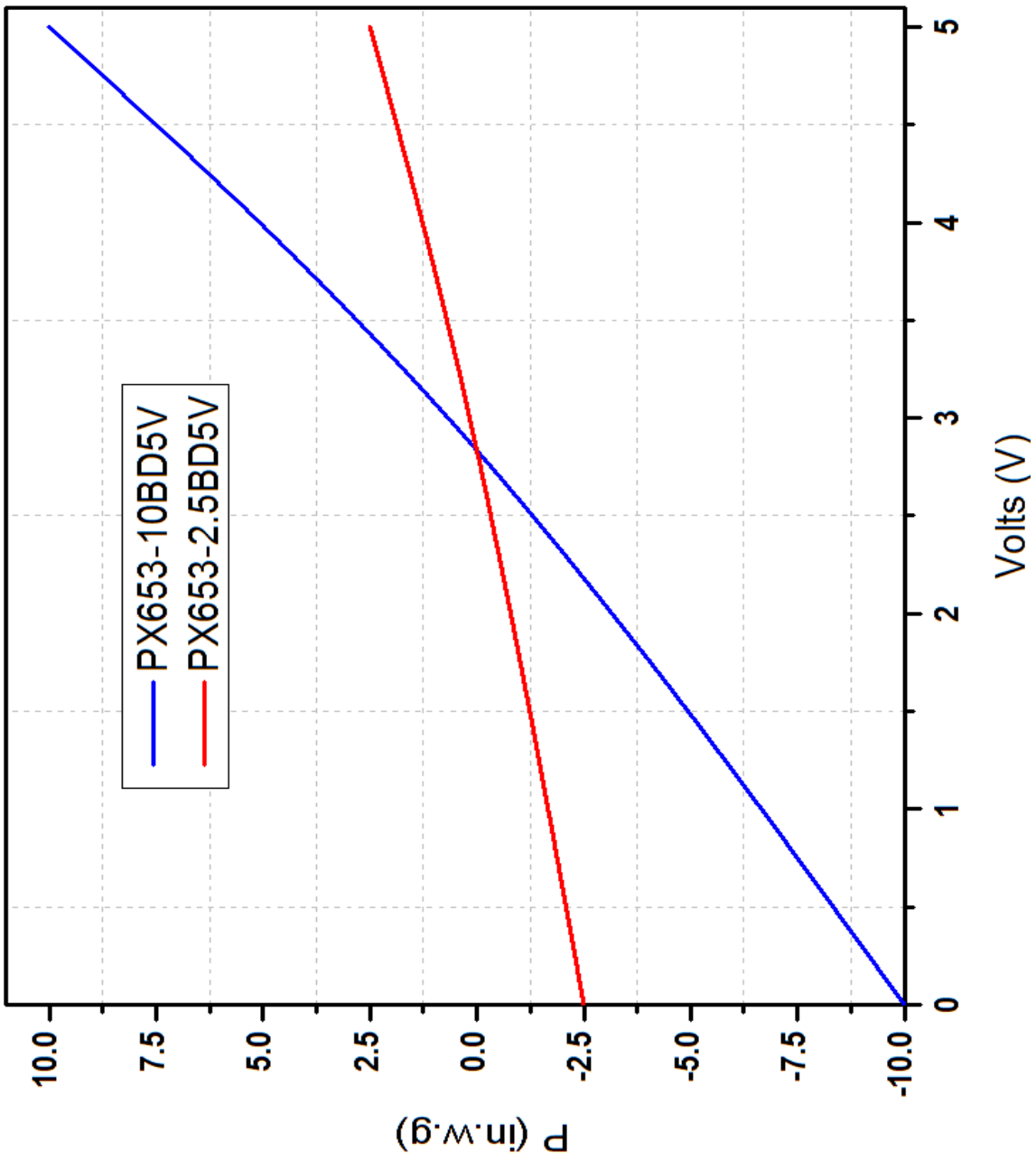

Figure 39: Pressure transducer conversion

Appendix C

CP35 Blade Profile Coordinates

CP 35 FAN BLADE COORDINATES								
R = 20.88 mm			R = 21.67107 mm			R = 23.374 mm		
θ = 35.3 degree			θ = 33.5			θ = 28.6 degree		
X	Y	Z	X	Y	Z	X	Y	Z
9.480238	3.016417	8	9.935567	2.990266	14	10.97399	2.797236	20
9.418286	2.983489	8	9.87032	2.958063	14	10.90135	2.776088	20
9.237666	2.883176	8	9.679941	2.859701	14	10.68841	2.709596	20
8.953071	2.71117	8	9.379487	2.690263	14	10.34925	2.58921	20
8.58577	2.461286	8	8.990746	2.44268	14	9.904322	2.402614	20
8.159278	2.127006	8	8.537822	2.109473	14	9.376464	2.136516	20
7.69427	1.703731	8	8.041947	1.685243	14	8.786273	1.780322	20
7.203572	1.191723	8	7.516395	1.169881	14	8.147603	1.330401	20
6.688115	0.599602	8	6.962412	0.572308	14	7.464023	0.794554	20
6.134698	-0.05192	8	6.367031	-0.08559	14	6.726933	0.19613	20
5.525656	-0.7353	8	5.712889	-0.77472	14	5.92414	-0.43369	20
4.861059	-1.43563	8	5.000557	-1.47961	14	5.059266	-1.08036	20
4.145278	-2.14109	8	4.234954	-2.18818	14	4.139797	-1.73314	20
3.383722	-2.8406	8	3.422055	-2.88906	14	3.17415	-2.38187	20
2.582885	-3.52398	8	2.568927	-3.57195	14	2.171648	-3.01721	20
1.750353	-4.18226	8	1.683734	-4.22775	14	1.14248	-3.63084	20
0.895884	-4.8069	8	0.776874	-4.84794	14	0.098548	-4.21499	20
0.032611	-5.37674	8	-0.13737	-5.41102	14	-0.94475	-4.7521	20
-0.84354	-5.88972	8	-1.06312	-5.91468	14	-1.98676	-5.23796	20
-1.72065	-6.34399	8	-1.98795	-6.3574	14	-3.01439	-5.67056	20

-2.58584	-6.73955	8	-2.89849	-6.73958	14	-4.01409	-6.04953	20
-3.4255	-7.07797	8	-3.78069	-7.06332	14	-4.97207	-6.37601	20
-4.22565	-7.3622	8	-4.62012	-7.33212	14	-5.87457	-6.65237	20
-4.97194	-7.59741	8	-5.40207	-7.55177	14	-6.70802	-6.88252	20
-5.64865	-7.79676	8	-6.1107	-7.73634	14	-7.45779	-7.07837	20
-6.24112	-7.97644	8	-6.7313	-7.90314	14	-8.10982	-7.25708	20
-6.73673	-8.15198	8	-7.25127	-8.06871	14	-8.65211	-7.43512	20
-7.12473	-8.33724	8	-7.65991	-8.24783	14	-9.07462	-7.62721	20
-7.39611	-8.54365	8	-7.94824	-8.45264	14	-9.36904	-7.84547	20
-7.54343	-8.77946	8	-8.10883	-8.69197	14	-9.52861	-8.09866	20
-7.56071	-9.04925	8	-8.13563	-8.9708	14	-9.54798	-8.39171	20
-7.45315	-9.29743	8	-8.03221	-9.23128	14	-9.4337	-8.66238	20
-7.22843	-9.46704	8	-7.80469	-9.41407	14	-9.19458	-8.8473	20
-6.88801	-9.55863	8	-7.45462	-9.51971	14	-8.83188	-8.94796	20
-6.43661	-9.57401	8	-6.98695	-9.54996	14	-8.34973	-8.9677	20
-5.88171	-9.51616	8	-6.40954	-9.50767	14	-7.75465	-8.91149	20
-5.2329	-9.38906	8	-5.73246	-9.39669	14	-7.05498	-8.78573	20
-4.5011	-9.19753	8	-4.96719	-9.22169	14	-6.26025	-8.59793	20
-3.69774	-8.94699	8	-4.12576	-8.98795	14	-5.3805	-8.35627	20
-2.835	-8.64052	8	-3.22089	-8.69819	14	-4.42722	-8.06436	20
-1.9274	-8.2747	8	-2.26755	-8.34833	14	-3.41435	-7.71917	20
-0.99005	-7.84615	8	-1.28132	-7.93437	14	-2.35644	-7.31813	20
-0.03792	-7.35301	8	-0.27766	-7.4539	14	-1.26818	-6.86001	20
0.91455	-6.79534	8	0.728458	-6.90651	14	-0.1641	-6.3452	20
1.853778	-6.17536	8	1.722871	-6.29406	14	0.941685	-5.77592	20

2.761503	-5.51185	8	2.686061	-5.63541	14	2.030034	-5.16695	20
3.643402	-4.81454	8	3.623568	-4.94085	14	3.10097	-4.52842	20
4.491335	-4.09097	8	4.526699	-4.21794	14	4.14398	-3.86741	20
5.29713	-3.35083	8	5.386663	-3.47648	14	5.148396	-3.19263	20
6.053841	-2.60503	8	6.195898	-2.72754	14	6.104473	-2.51386	20
6.755741	-1.8654	8	6.948079	-1.98321	14	7.003443	-1.8417	20
7.398268	-1.14445	8	7.638065	-1.25633	14	7.837536	-1.18732	20
7.974601	-0.45228	8	8.258462	-0.55715	14	8.597037	-0.55868	20
8.461997	0.213607	8	8.785827	0.117614	14	9.258273	0.052935	20
8.843737	0.849601	8	9.202744	0.764718	14	9.802942	0.649083	20
9.118493	1.441431	8	9.507376	1.369416	14	10.22657	1.217078	20
9.297807	1.968604	8	9.710984	1.910108	14	10.53649	1.734735	20
9.401757	2.408553	8	9.833595	2.362777	14	10.74819	2.17541	20
9.453691	2.740147	8	9.898664	2.704789	14	10.8807	2.512767	20
9.474921	2.946409	8	9.927675	2.917881	14	10.95179	2.72486	20
9.480238	3.016417	8	9.935567	2.990266	14	10.97399	2.797236	20

CP 35 FAN BLADE COORDINATES								
R = 24.766 mm			R = 27.6089 mm			R = 32.34289 mm		
θ = 23.1 degree			θ = 20.9 degree			θ = 18.5 degree		
X	Y	Z	X	Y	Z	X	Y	Z
11.88657	2.429155	26	14.63993	2.954743	29	20.35433	4.10502	34
11.8118	2.41547	26	14.55801	2.942636	29	20.26117	4.089853	34
11.5913	2.370978	26	14.31582	2.902605	29	19.98498	4.040801	34
11.23592	2.28606	26	13.9235	2.824266	29	19.53519	3.947936	34
10.76154	2.146898	26	13.39604	2.692721	29	18.92584	3.797084	34
10.18623	1.938592	26	12.75068	2.491903	29	18.17334	3.573107	34
9.52691	1.649104	26	12.00398	2.208778	29	17.29393	3.263997	34
8.796162	1.273621	26	11.16894	1.837917	29	16.30123	2.865312	34
7.999698	0.818842	26	10.25278	1.385906	29	15.20425	2.384393	34
7.135029	0.306616	26	9.25564	0.874974	29	14.00641	1.843789	34
6.197482	-0.23403	26	8.17594	0.33462	29	12.71	1.273043	34
5.193842	-0.79043	26	7.02247	-0.22259	29	11.32651	0.685256	34
4.13385	-1.35355	26	5.806814	-0.7878	29	9.870083	0.089911	34
3.028078	-1.91479	26	4.541416	-1.35253	29	8.355824	-0.50395	34
1.887855	-2.46619	26	3.239483	-1.90889	29	6.799692	-1.08795	34
0.725182	-3.0006	26	1.914868	-2.44972	29	5.218341	-1.65452	34
-0.44677	-3.51146	26	0.58245	-2.96852	29	3.629409	-2.19686	34
-1.61246	-3.98533	26	-0.74094	-3.4526	29	2.052121	-2.70184	34
-2.76613	-4.41689	26	-2.04664	-3.89605	29	0.498496	-3.16262	34
-3.89404	-4.80406	26	-3.31944	-4.2965	29	-1.01355	-3.57689	34
-4.98237	-5.14613	26	-4.54412	-4.65287	29	-2.46623	-3.94379	34
-6.01737	-5.44362	26	-5.70576	-4.96528	29	-3.84215	-4.26371	34
-6.98566	-5.6981	26	-6.78989	-5.23484	29	-5.12457	-4.53817	34

-7.8744	-5.91193	26	-7.78276	-5.46345	29	-6.29764	-4.7695	34
-8.67116	-6.09	26	-8.67151	-5.65398	29	-7.34665	-4.96064	34
-9.36264	-6.24786	26	-9.44266	-5.81885	29	-8.25791	-5.11726	34
-9.93692	-6.40375	26	-10.0831	-5.9788	29	-9.017	-5.26109	34
-10.3842	-6.57402	26	-10.5819	-6.15278	29	-9.61118	-5.41822	34
-10.6966	-6.77218	26	-10.9305	-6.35648	29	-10.0305	-5.61037	34
-10.868	-7.0081	26	-11.1222	-6.60146	29	-10.2676	-5.85363	34
-10.8937	-7.28747	26	-11.1524	-6.8944	29	-10.3172	-6.15753	34
-10.7814	-7.54466	26	-11.0302	-7.16245	29	-10.1881	-6.43717	34
-10.5407	-7.71319	26	-10.7669	-7.33196	29	-9.89134	-6.60676	34
-10.1728	-7.79614	26	-10.3639	-7.40736	29	-9.42879	-6.67323	34
-9.68139	-7.79929	26	-9.82465	-7.39656	29	-8.80449	-6.64851	34
-9.07191	-7.73079	26	-9.15459	-7.31056	29	-8.02434	-6.54891	34
-8.35125	-7.60074	26	-8.36031	-7.16286	29	-7.09547	-6.39424	34
-7.52715	-7.42073	26	-7.4493	-6.96845	29	-6.02699	-6.19954	34
-6.60855	-7.19972	26	-6.43158	-6.73412	29	-4.83203	-5.96389	34
-5.6074	-6.9366	26	-5.32014	-6.45777	29	-3.52553	-5.68429	34
-4.53694	-6.62892	26	-4.12905	-6.13744	29	-2.12362	-5.35832	34
-3.41102	-6.27503	26	-2.87313	-5.77198	29	-0.64337	-4.98446	34
-2.24388	-5.8744	26	-1.56773	-5.36127	29	0.897477	-4.56229	34
-1.04989	-5.42775	26	-0.22846	-4.90642	29	2.480785	-4.09271	34
0.156657	-4.93727	26	1.129012	-4.40987	29	4.088254	-3.57807	34
1.357875	-4.41367	26	2.48591	-3.88156	29	5.698896	-3.02832	34
2.548286	-3.86651	26	3.833787	-3.33122	29	7.300903	-2.45435	34
3.71565	-3.30199	26	5.158548	-2.76511	29	8.877336	-1.86274	34

4.847658	-2.72743	26	6.446084	-2.1905	29	10.41131	-1.26114	34
5.93269	-2.15101	26	7.682945	-1.61543	29	11.88666	-0.65807	34
6.959918	-1.58153	26	8.856465	-1.04853	29	13.28806	-0.06267	34
7.919374	-1.02825	26	9.954861	-0.49882	29	14.60119	0.515443	34
8.799925	-0.49722	26	10.96546	0.028025	29	15.81127	1.069863	34
9.580849	0.02196	26	11.86726	0.543401	29	16.89669	1.610725	34
10.24551	0.53311	26	12.64312	1.052049	29	17.83948	2.14181	34
10.78742	1.026013	26	13.28516	1.544181	29	18.62994	2.652862	34
11.20884	1.48056	26	13.79359	1.999582	29	19.2657	3.123533	34
11.51834	1.871495	26	14.17446	2.392456	29	19.74984	3.528075	34
11.72747	2.173184	26	14.4368	2.696384	29	20.0885	3.840198	34
11.84753	2.363895	26	14.58975	2.888832	29	20.28834	4.037502	34
11.88657	2.429155	26	14.63993	2.954743	29	20.35433	4.10502	34